

**An-Najah National University**

**Faculty of Graduate Studies**

**Structural, Elastic and Electronic Properties of:  
KI and RbI Compounds**

**By**

**Zainab "Mohammed Bakir" Mualla**

**Supervisors**

**Prof. Dr. Mohammed Abu-Jafar**

**Dr. Ahmed Bassalat**

**This Thesis is Submitted in Partial Fulfillment of the Requirements for  
the Degree of Master of Physics, Faculty of Graduate Studies, An-Najah  
National University, Nablus - Palestine**

**2021**

# Structural, Elastic and Electronic Properties of: KI and RbI Compounds

By

Zainab "Mohammed Bakir" Mualla

This Thesis was Defended Successfully on 29/12/2021 and approved by:

Defense Committee Members:

Signature

1. Prof. Dr. Mohammed Abu Jafar /Supervisor

Mohammed Abu Jafar

2. Dr. Ahmed Bassalat /Co-Supervisor

Ahmed Bassalat

3. Dr. Raed Jaradat/External Examiner

Raed Jaradat

4. Dr. Mahmoud Farout /Internal Examiner

Mahmoud Farout

### III

## **Dedication**

To my dear mother and father who encouraged me to keep learning. To my sisters and brothers who inspire me to do my best.

To my second family for their care and support.

To my husband, Asem, for motivating and supporting me through the hard times.

## **Acknowledgment**

My great appreciation and gratitude to my dear supervisors: Prof. Dr. Mohammed Abu Jafar and Dr. Ahmed Bassalat for their valuable mentorship, guidance, support and patience throughout this work .

I would like to express my gratitude for all the teachers and staff of the physics department at An-Najah National University for their hard work and for facilitating working on this thesis.

My appreciation also goes to the members of the jury: Dr.Raed Jaradat and Dr. Mahmoud Farout for their valuable feedback.

أنا الموقع أدناه مقدم الرسالة التي تحمل عنوان

## Structural, Elastic and Electronic Properties of: KI and RbI Compounds

أقر بأن ما اشتملت عليه هذه الرسالة إنما هي نتاج جهدي الخاص، باستثناء ما تمت الإشارة إليه حيثما ورد، وأن هذه الرسالة ككل، أو أي جزء منها لم يقدم من قبل لنيل أي درجة أو لقب علمي أو بحث لدى أي مؤسسة تعليمية أو بحثية أخرى.

### Declaration

The work provided in this thesis, unless otherwise referenced, is the researcher's own work, and has not been submitted elsewhere for any other degree or qualification

Student's name:

اسم الطالب: زينب محمد بكر مهلا

Signature:

التوقيع: زينب مهلا

Date:

التاريخ: 29/12/2021

## Table of Contents

Dedication .....	III
Acknowledgment.....	IV
Table of Contents .....	VI
List of Tables .....	VIII
List of Figures.....	X
List of abbreviations.....	XIII
Abstract .....	XV
Chapter One: Introduction.....	1
Chapter Two: Theoretical background .....	6
2.1: The many-body Schrodinger equation.....	6
2.2: Basic approximations to the Schrodinger equation .....	8
2.3: Density Functional Theory .....	10
2.4: Full-potential linearized augmented plane wave method (FP-LAPW) .....	19
Chapter Three: Lattice structures.....	24
3.1: Rocksalt (RS) structure .....	26
3.2: Cesium chloride (CsCl) structure .....	26
3.3: Zincblende (ZB) structure.....	27
3.4: Nickel Arsenide (NiAs) structure .....	27
3.5: Wurtzite (WZ) structure.....	28
Chapter Four: Methodology.....	29
4.1: WIEN2k software package .....	29
4.2: Structural properties.....	30
4.2.1: Structural properties for cubic structures.....	31
4.2.2: Structural properties for NiAs structure .....	32
4.2.3: Structural properties for WZ structure.....	33
4.2.4: Phase transformation and transition pressure .....	34
4.3: Electronic properties .....	37
4.3.1: Band structure .....	37
4.3.2: Electron density of state (DOS).....	38

4.3.3: Energy band gap .....	38
4.4: Elastic properties.....	39
4.4.1: Stress, strain and elastic constants .....	39
4.4.2: Stability conditions .....	41
4.4.3: Elastic moduli .....	41
Chapter Five: Results and analysis .....	47
5.1: Potassium iodide (KI) compound .....	47
5.1.1: Structural properties.....	47
5.1.2: Phase transformations .....	49
5.1.3: Electronic properties .....	51
5.1.4: Elastic properties .....	57
5.2: Rubidium Iodide (RbI) compound.....	60
5.2.1: Structural properties.....	60
5.2.2: Phase transition .....	62
5.2.3: Electronic properties .....	64
5.2.4: Elastic properties .....	70
Chapter Six: Conclusion.....	74
References .....	76
المخلص .....	ب

## List of Tables

Table (5.1.1): The structural properties of KI in RS, CsCl and ZB structures with other available experimental and theoretical results. ....	48
Table (5.1.2): The structural properties of KI in NiAs and WZ structures	49
Table (5.1.3): Transition pressures for the transition of KI between various structures along other available experimental and theoretical results .....	51
Table (5.1.4): Energy band gap (in eV) for KI in the examined structures, using the approximations GGA and mBJ, with other available experimental and theoretical results .....	55
Table (5.1.5): The elastic constants ( $C_{11}$ , $C_{12}$ and $C_{44}$ ) and the bulk modulus calculated by Hill's approximation for KI in RS, CsCl and ZB structures, all in (GPa) .....	58
Table (5.1.6): The elastic constants ( $C_{11}$ , $C_{12}$ , $C_{13}$ , $C_{33}$ and $C_{55}$ ) and the bulk modulus calculated by Hill's approximation for KI in WZ structures, all in (GPa) .....	58
Table (5.1.7): The calculated Hill's Shear modulus ( $S_H$ ), Young's modulus ( $Y_H$ ) in (GPa), Poisson's ratio ( $\nu_H$ ), the anisotropic ratio (A), B/S ratio, Cauchy pressure ( $P_C$ ) in (GPa), the compressibility ( $\beta$ ) in (1/GPa), and the Hardness (H), for KI compound in RS, CsCl, ZB and WZ structures.....	59
Table (5.2.1): Structural properties of RbI in RS, CsCl and ZB structures with other available experimental and theoretical results .....	61
Table (5.2.2): The structural properties of RbI in NiAs and WZ structures .....	61
Table (5.2.3): Transition pressures for the transition of RbI between various structures along other available experimental and theoretical results .....	63

Table (5.2.4): Energy band gap (in eV) for RbI using GGA and mBJ approximations, with other available experimental and theoretical results .....	67
Table (5.2.5): The elastic constants ( $C_{11}$ , $C_{12}$ and $C_{44}$ ) and the bulk modulus calculated by Hill's approximation for RbI in RS, CsCl and ZB structures, all in (GPa). .....	71
Table (5.2.6): Elastic properties for RbI in NiAs and WZ structures .....	71
Table (5.2.7): The calculated Hill's Shear modulus ( $S_H$ ), Young's modulus ( $Y_H$ ) in (GPa), Poisson's ratio ( $\nu_H$ ), the anisotropic ratio (A), B/S ratio, Cauchy pressure ( $P_C$ ) in (GPa), the compressibility ( $\beta$ ) in (1/GPa), and the Hardness (H), for RbI compound in RS, CsCl, ZB and WZ structures.....	72

## List of Figures

Figure (1.1): Alkali metals and halides in the periodic table .....	1
Figure (2.1): Flow chart for the self-consistent field cycles to solve KS equations. ....	15
Figure (2.2): Division of a unit cell into two regions: (I) are muffin-tin regions, and (II) is the interstitial region, for a system of two atoms. ....	20
Figure (3.1): Representation of simple cubic unit cells in a solid with periodic structure.....	24
Figure (3.2): Lattice constants: a, b and c for a unit cell. The angles between the lattice vectors are: $\alpha$ , $\beta$ and $\gamma$ .....	25
Figure (3.3): Rocksalt structure (RS) .....	26
Figure (3.4): Cesium Chloride structure (CsCl) .....	26
Figure (3.5): Zincblende structure (ZB).....	27
Figure (3.6): Nickle arsenide structure (NiAs) .....	28
Figure (3.7): Wurtzite structure (WZ).....	28
Figure (4.1): WIEN2k software package logo .....	29
Figure (4.2): High pressure effect on lattice structure of KI. ....	34
Figure (4.3): Extracting the transition pressure (between the structures S1 and S2) from EOS graphs .....	35
Figure (4.4): Calculating transition pressure using the enthalpy. ....	36
Figure (4.5): First brillouin zone for FCC lattice.....	38
Figure (4.6): Poisson's ratio in terms of strain .....	45
Figure (5.1.1): Energy (in Ry) calculated at each volume versus the volume (in a.u. <sup>3</sup> ) for KI in RS, CsCl, ZB, NiAs and WZ structures .	49
Figure (5.1.2): Enthalpy H (in Ry) versus pressure P (in GPa) for KI phase transformations using PBE-GGA approximation.....	50

Figure (5.1.3.a): Band structure for KI in the cubic structures RS, CsCl and ZB using the approximation GGA and mBJ. .... 53

Figure (5.1.3.b): Band structure for KI in the hexagonal structures NiAs and WZ using the approximation GGA and mBJ. .... 54

Figure (5.1.4): Density of states (DOS) of KI in the RS structure, using GGA approximation ..... 55

Figure (5.1.5): Density of states (DOS) of KI in the CsCl structure, using GGA approximation ..... 56

Figure (5.1.6): Density of states (DOS) of KI in the ZB structure, using GGA approximation ..... 56

Figure (5.1.7): Density of states (DOS) of KI in the NiAs structure, using GGA approximation ..... 57

Figure (5.1.8): Density of states (DOS) of KI in the WZ structure, using GGA approximation ..... 57

Figure (5.2.1): Energy (in Ry) calculated at each volume versus the volume (in a.u.<sup>3</sup>) for RbI in RS, CsCl, ZB, NiAs and WZ structures 62

Figure (5.2.2): Enthalpy H (in Ry) versus pressure P (in GPa) for RbI phase transformations using PBE-GGA approximation..... 63

Figure (5.2.3.a): Band structures for RbI in the cubic structures RS, CsCl and ZB using the approximation GGA and mBJ. .... 65

Figure (5.2.3.b): Band structure for RbI in the hexagonal structures NiAs and WZ using the approximation GGA and mBJ. .... 66

Figure (5.2.4): Density of states (DOS) for RbI in RS structure using GGA approximation ..... 68

Figure (5.2.5): Density of states (DOS) for RbI in CsCl structure using GGA approximation ..... 69

Figure (5.2.6): Density of states (DOS) for RbI in ZB structure using GGA approximation ..... 69

Figure (5.2.7): Density of states (DOS) for RbI in NiAs structure using GGA approximation .....	70
Figure (5.2.8): Density of states (DOS) for RbI in WZ structure using GGA approximation   .....	70

**List of abbreviations**

<b>Abbreviation</b>	<b>Meaning</b>
KI	Potassium iodide
RbI	Rubidium iodide
RS	Rocksalt
CsCl	Cesium chloride
ZB	Zinc blende
NiAs	Nickle arsenide
WZ	Wurtzite
DFT	Density functional theory
XC	Exchange correlation
KS	Kohn Sham
LDA	Local density approximation
GGA	Generalized gradient approximation
PBE	Perdew-Burke-Ernzerhof approximation
mBJ	modified Becke Johnson approximation
PW	Plane waves
APW	Augmented plane wave method
LAPW	Linearized augmented plane wave method
FP-LAPW	Full-potential linearized augmented plane wave method
MT	Muffin-tin model
$R_{MT}$	Radius of muffin-tin spheres
BZ	Brillouin zone
EOS	Equation of state
SCF	Self-consistent field cycles
a, b, c	Lattice constants

## XIV

u	Internal parameter for the hexagonal structures
B	Bulk modulus
$P_t$	Transition pressure
$V_0$	Equilibrium volume
$E_0$	Energy at equilibrium volume
DOS	Density of states
MVB	Maximum valence band
MCB	Minimum conduction band
BS	Band structure
$E_g$	Energy band gap
$E_F$	Fermi energy
S	Shear modulus
H	Hardness
Y	Young modulus
$\nu$	Poisson's ratio
A	Anisotropic factor
$C_s$	Cauchy's pressure
$\beta$	Compressibility

# **Structural, Elastic and Electronic Properties of: KI and RbI Compounds**

**By  
Zainab Mualla**

**Supervisors  
Prof. Dr. Mohammed Abu-Jafar  
Dr. Ahmed Bassalat**

## **Abstract**

The structural, elastic, and electronic properties of potassium iodide (KI) and rubidium iodide (RbI) have been investigated using the full potential linearized augmented plane wave method (FP-LAPW) and the generalized gradient approximation (GGA) of the potential. The modified Becke Johnson approximation (mBJ) of the potential is used to improve the results of the electronic properties. The compounds KI and RbI are studied in the RS, CsCl, ZB, NiAs and WZ structures.

The structural parameters are found to be in a very good agreement with the available theoretical and experimental results. The RS structure is found to be the ground state for both compounds. Also, the band structure results for the compounds KI and RbI have indicated a wide-band gap semiconductor behavior in all the included structures. The overall values obtained for the bulk modulus were low, denoting weak resistance to fracturing.

The elastic constants are calculated for KI and RbI in RS, CsCl, ZB, NiAs and WZ structures and found to be stable according to Born's stability criteria. While the NiAs structure for RbI is found unstable. KI and RbI in all the included structures have shown ductile behavior, as well as an ionic

bonding nature. Moreover, all the structures showed anisotropic nature, except RbI in WZ, which gave anisotropy factor (A) of one (Isotropic). The stiffness of the compounds was investigated using the Poisson's ratio and Cauchy's pressure. The results for KI showed that CsCl is the stiffest structure, while for RbI, RS structure was found to be the stiffest.

## Chapter One

### Introduction

Alkali halides are electrically insulating salts that consist of alkali cations and halide anions; ions of the elements in group IA and VIIA in the periodic table, respectively, as illustrated in figure (1.1)

I	II															VIII
Li																F
Na																Cl
K																Br
Rb																I
Cs																At
Fr																Ts

**Figure (1.1): Alkali metals and halides in the periodic table**

In normal conditions, alkali halides are stable crystallized compounds of Rocksalt (RS) structure [1]. These compounds, including alkali iodides, have been fundamental compounds in solid state physics' research areas since the last century [2, 3, 4, 5, 6], as well as in recent years [7, 8, 9]. Alkali halides drew a lot of attention due to their interesting properties, such as the crystal structure transitions at high pressures. Among the alkali halides family, the compounds potassium iodide (KI) and rubidium iodide (RbI) are chosen for this work. Alkali iodides are well known compounds in the research community. For instance, Potassium iodide KI is included in many nanoscience research papers, such as single-walled carbon nanotubes [10]

Rubidium iodide RbI is used in optical industry due to its high transparency, especially in the infrared region [11]. In addition, both compounds are used in chemical reactions and have medical applications such as the usage of KI in thyroid treatments.

Moreover, the compounds KI and RbI are studied, experimentally and theoretically, in RS structure on many occasions, but seldom considered in other structures. For instance, for RS structure, the lattice constant "a" was found experimentally to be 7.094 Å [7] and 7.342 Å for KI and RbI, respectively, and 4.33 Å for RbI in CsCl structure [12]. The bulk modulus (B) for KI was also found experimentally by Weir et al. [13] to be 11.6 GPa, and according to the theoretical calculations done by Cortona et al., B has the value 13.8 GPa [14]. While for RbI in RS structure, the experiments held by Chang et al. [15] and Ghafelehbashii et al. [16] using the ultrasonic techniques found the bulk modulus to be 11.094 GPa and 11.07 GPa, respectively. Meanwhile, theoretical calculations reported that the bulk modulus for RbI in RS structure is 12.2 GPa [14].

One of the most interesting features of alkali halides is their ability to change structure under relatively low pressure. The pressure at which a structural phase transformation occurs is called the transition pressure ( $P_t$ ). Experiments observed that a phase transition from RS structure (B1) to CsCl structure (B2) occurs at relatively low pressures. Transition pressure values were found to be 1.73 GPa by Barsch et al. [17], and 1.9 GPa by Asaumi et al. [5] for KI. Regarding RbI, the transition pressure was found to be 0.35

GPa, 0.38 GPa, and 0.4 GPa by Asenbaum et al. [18], Jacobs et al. [12], and Asaumi et al. [5], respectively. On the other hand, Sarkar et al. calculated the transition pressure for RbI to be 0.23 GPa [19].

The electronic properties have been investigated for KI and RbI in RS structure. The energy band gap ( $E_g$ ) values were observed from absorption spectra graphs by Teegarden et al. [20], with the values 6.1 eV and 6 eV for KI and RbI in RS structure, respectively. Another experimental work was done by Hopfield et al. [21], giving an energy band gap of 6.34 eV for KI in RS structure. Calculations were also performed to calculate the energy band gap for both KI and RbI in RS, some of the values found for KI are 5.984 eV [7] using the full potential linearized muffin-tin orbital (FP-LMTO) method, 4.26 eV [22] using the first-principles linearized augmented-plane-wave band method, and 5.951 eV using the modified Becke Johnson (mBJ) approximation of the potential [23]. These energy band gap values indicate a wide-band gap semiconducting behavior of the two compounds: RbI and KI in, RS structure.

The elastic properties for any compound can be represented using many elastic constants and moduli such as the bulk and young moduli. However, the most basic elastic constants are:  $C_{11}$ ,  $C_{12}$ , and  $C_{44}$  for the cubic structures, with the additional two elastic constants:  $C_{13}$  and  $C_{33}$  for the hexagonal structures. The elastic constants for KI and RbI were considered on many occasions, using experimental and theoretical methods. Norwood and Briscoe measured the elastic constants for KI using the ultrasonic pulse

technique, and were able to find that  $C_{11}$ ,  $C_{12}$  and  $C_{44}$  have the values 27.1, 4.5, 3.64 GPa, respectively [24]. The reported values of  $C_{11}$ ,  $C_{12}$  and  $C_{44}$  by Bridgman are 33.2, 5.78 and 6.2 GPa [25]. On the other hand, Sarkar and Sengupta used a theoretical approach to calculate the elastic constants, using the homogenous deformation method as a basis to their calculations, the values obtained by this method were 31.7, 3.2, and 4.2 GPa for  $C_{11}$ ,  $C_{12}$  and  $C_{44}$ , respectively [19]. Finally, the Young modulus was calculated to be 15.3 GPa by Gahn et al. [26]. Similarly, RbI elastic constants were experimentally measured and calculated theoretically on many occasions. For instance, measurements of the elastic constants reported the values of  $C_{11}$ ,  $C_{12}$  and  $C_{44}$  for RbI in RS structure to be (in order): 25.55, 3.45, and 2.76 GPa by Aenbaum et al. [18], 25.5, 3.4 and 2.773 GPa by Lewis et al. [4], and 25.56, 3.82 and 2.78 GPa by Ghafelehbashi [16]. Sarkar and Sengupta's calculations gave the values 25.8, 3.3 and 3.6 GPa for the elastic constants  $C_{11}$ ,  $C_{12}$  and  $C_{44}$ , respectively [19]. The young modulus value was calculated to be 13 GPa [26]. All the previous results of the elastic constants are for the RS structure, where no results were found for the other structures regarding the elastic properties.

This work aims to extend the knowledge of the structural, elastic, and electronic properties of the compounds: KI and RbI, in the structures: Rock salt (RS), cesium chloride (CsCl), zincblende (ZB), nickel arsenide (NiAs) and wurzite (WZ).

Multiple theoretical approaches and approximations were used to study KI and RbI properties. Likewise, many experiments were performed on these alkali iodides to study their properties. However, Alkali halides' properties are rarely studied using the FP-LAPW method. This approach has the advantage of considering all electrons in the muffin tin potential (hence the name: full potential). As a result, more accurate results can be achieved when applying the full potential to Schrodinger's equations.

## Chapter Two

### Theoretical background

#### 2.1: The many-body Schrodinger equation

In 1926, Schrodinger published a paper where he used his famous equation to solve the simplest system at quantum scale: the hydrogen atom [27]. He was able to give competent results compared to the Bohr model. Since then, attempts have been made to solve more complicated systems using the Schrodinger equation.

One of the most complicated systems to solve is the solids with periodic structure with multi-atomic unit cells systems, due to the fact that more particles require more variables and more complicated calculations. Here, quantum mechanics can be used, and the associated time-independent Schrodinger equation is: [28]

$$\hat{H}\psi = E\psi \quad (2.1)$$

Where H is the Hamiltonian of the multi-atomic unit cell,  $\psi$  is the superposition wave function of all atoms in the unit cell, and E is the total energy for the system.

The Hamiltonian H can be written as:

$$\hat{H} = T_n + T_e + V_{en} + V_{ee} + V_{nn} \quad (2.2)$$

Where  $T_n$  is the kinetic energy of the nuclei,  $T_e$  is the kinetic energy of the electrons,  $V_{en}$  is the Coulomb interaction potential between the electrons and the nuclei,  $V_{ee}$  is the coulomb interaction potential between the electrons and  $V_{nn}$  is the Coulomb interaction potential between the nuclei.

The Hamiltonian is given in details in equation (2.3):

$$\begin{aligned} \hat{H} = & -\frac{\hbar^2}{2} \sum_i \frac{\nabla_{\vec{R}_i}^2}{M_i} - \frac{\hbar^2}{2} \sum_i \frac{\nabla_{\vec{r}_i}^2}{m_i} - \frac{1}{4\pi\epsilon_0} \sum_{ij} \frac{e^2 Z_i}{|\vec{R}_i - \vec{r}_j|} + \frac{1}{8\pi\epsilon_0} \sum_{i \neq j} \frac{e^2}{|\vec{r}_i - \vec{r}_j|} + \\ & + \frac{1}{8\pi\epsilon_0} \sum_{i \neq j} \frac{e^2 Z_i Z_j}{|\vec{R}_i - \vec{R}_j|}, \end{aligned} \quad (2.3)$$

where  $\hat{H}$  is the Hamiltonian of the system,  $\hbar$  is Plank's constant,  $R_i$  is the position of atom  $i$ ,  $M_i$  is the mass of the atom  $i$ ,  $r_j$  is the position of the electron  $j$ ,  $m_j$  is the mass of the electron  $j$ ,  $Z_i$  is the atomic number of the atom  $i$ ,  $e$  is the electron's charge and  $\epsilon_0$  is the permittivity of free space.

The number of variables and degrees of freedom in the above equations depends on the number of nuclei and electrons in the solid under examination, which is extremely high. This leads to complicated calculations, which makes getting exact solutions almost impossible.

To study such systems, approximations are required to simplify the Hamiltonian to help solving the Schrodinger equation. Different approximations will be presented in section 2.

## 2.2: Basic approximations to the Schrodinger equation

### a- The Born-Oppenheimer approximation

Born-Oppenheimer approximation is a simple, yet a very useful approximation. Born and Oppenheimer stated that the nuclei are much heavier than the electrons and have very limited motion (low mobility). Therefore, the nuclei kinetic energy is immensely lower than the electrons, which can be neglected [29]. Therefore, the kinetic energy term of the nuclei is excluded and their electric interaction with the electrons is considered an external constant potential function affecting the electrons.

Considering equations (2.2) and (2.3) and using the Born-Oppenheimer approximation, the first term is eliminated, which leads to a simpler form of the Hamiltonian: [29]

$$H = T_e + V_{ee} + V_{ext} \quad (2.4)$$

This approximation reduces the number of degrees of freedom to  $3N_e$ , where  $N_e$  is the number of electrons in the system. This simplification, however, is not enough to solve the Schrodinger equation of the many-body systems.

### b- Hartree and Hartree-Fock Approximations

In Hartree approximation [30], the electrons are assumed to be independent and do not interact with each other. This affects the representation of the total wave function for the electrons as follows:

$$\Psi(r_1, r_2, r_3, \dots, r_N) = \Psi_1(r_1)\Psi_2(r_2)\Psi_3(r_3) \dots \Psi_N(r_N), \quad (2.5)$$

where  $\Psi_N(r_N)$  is the single electron wave function.

The electron-electron potential is replaced by an effective potential called the Hartree potential:

$$V_H = \frac{1}{8\pi\epsilon_0} \sum_{ij} \frac{|\psi(r_i)|^2 |\psi(r_j)|^2 d^3r_i d^3r_j}{|\vec{r}_i - \vec{r}_j|}. \quad (2.6)$$

The Hamiltonian gets the form:

$$\hat{H} = T_e + V_{ext} + V_H, \quad (2.7)$$

where  $T_e$  is the electrons' kinetic energy,  $V_{ext}$  is the nuclei potential affecting the electrons and  $V_H$  is the Hartree potential.

Hartree's mathematical representation assumes that electrons can occupy the same state since they do not interact, therefore, cannot "detect" the existence of other electrons. This contradicts with Pauli Exclusion Principle which states that no two fermions can occupy the same quantum state and have the same quantum numbers. To solve this issue, Fock stated that the total wavefunction of the electrons should be antisymmetric and represented by the Slater determinant, as shown in equation (2.8). Therefore, the permutation symmetry of the wavefunction was taken into account. [31]

$$\Psi(r_1, r_2, r_3, \dots, r_N) = \frac{1}{\sqrt{N}} \begin{vmatrix} \Psi_1(r_1) & \dots & \Psi_N(r_1) \\ \vdots & \ddots & \vdots \\ \Psi_1(r_N) & \dots & \Psi_N(r_N) \end{vmatrix}, \quad (2.8)$$

where  $N$  is the number of electrons in the system, and  $\Psi_i(r_j)$  is the  $i^{\text{th}}$  wavefunction for the  $j^{\text{th}}$  electron. This modification started a new chapter in

studying large systems with periodic potentials, where a quantum contribution to the Hamiltonian is included, represented by the exchange potential.

### 2.3: Density Functional Theory

The previous approximations include at least  $3N_e$  degrees of freedom, which leads to very difficult, complicated, and expensive calculations. This led to the development of new approaches to the problem. Among them is the density functional theory (DFT), initiated by Hohenberg and Kohn's theorem [32]. This theory observes the system as an inhomogeneous electron gas in order to solve Schrodinger's equation.

DFT is an interpretation of the multi-atomic systems in which the number of variables describing the interacting electrons is reduced. This can be obtained by considering the electron density, which is a function of space and time, then finding the energy as a functional of the density. The electron density is a scalar function as shown:

$$\rho = \rho(\vec{r}_1, \vec{r}_2, \dots, \vec{r}_i, t), \quad (2.9)$$

where  $\rho$  is the electron density function,  $\vec{r}_i$  is the position of the electron  $i$ , and  $t$  is the time.

DFT is established due to the great efforts of many physicists. Hohenberg and Kohn were the first to set the foundation stone of DFT.

### a) Hohenberg-Kohn theorem

The first appearance of the electron density was in 1927 by Thomas and Fermi [33]. They considered the electrons as a free gas that exists as a distribution around the nuclei. In 1964, Hohenberg and Kohn published their theorem, which used the electron density as an efficient tool to reduce the number of variables when working with many-body problems. In their theorem, Hohenberg and Kohn stated the relation between the total wavefunction of the electrons and the electron density to be as bellow: [32]

$$\rho(r) = N \int |\Psi(r_1, r_2, r_3, \dots, r_N)|^2 dr_2 dr_3 \dots dr_N . \quad (2.10)$$

In DFT, the energy is a unique functional of the electrons' density  $E[\rho]$ , where the ground state energy is the minimum value of the functional  $E[\rho]$ , and the associated  $\rho$  is the ground-state electron density. [32]

DFT divides the total energy into several terms; the first four terms consider a classical non-interacting system of electrons (the same formula for Hartree approximation), with an additional last term that gives the quantum-mechanical corrections needed to match the real total energy. Therefore, the total energy is written as:

$$E(\rho) = T_e(\rho) + E_{en}(\rho) + E_{nn}(\rho) + E_H(\rho) + E_{XC}(\rho) , \quad (2.11)$$

where  $T_e(\rho)$  is the kinetic energy of the non-interacting electrons,  $E_{en}(\rho)$  is the interaction energy between the electrons and nuclei,  $E_{nn}(\rho)$  is the nuclei interactions,  $E_{XC}(\rho)$  is the exchange-correlation energy, and  $E_H(\rho)$  is the

Hartree energy which represents the interactions of the electrons. Hartree energy can be represented by [34]:

$$E_H(\rho) = \frac{e^2}{2} \int d^3r d^3\hat{r} \frac{\rho(\vec{r})\rho(\vec{\hat{r}})}{|\vec{r}-\vec{\hat{r}}|}. \quad (2.12)$$

The exchange-correlation (XC) functional is the sum of a correlation functional and exchange functional:

$$E_{XC} = E_X + E_C, \quad (2.13)$$

Such that  $E_X$  is the exchange energy that comes from Pauli Exclusion Principle, and  $E_C$  is the correlation energy that originates from the interaction of electrons having the same spin [35].

## b) Kohn-Sham theory

Trial functions have come in handy on many occasions in physics. Kohn and Sham used them in their theorem in 1965. [36]

Kohn and Sham proposed the assumption that for a system of interacting electrons, the ground state electron density should be equal to the electron density of a system of non-interacting electrons with the same particles' arrangement. This theorem made DFT an efficient computational tool to solve the problem of many-electron systems. [36]

According to the variational principle, a set of effective one-particle Schrodinger equations must be solved. In our system of solids, these are called the Kohn-Sham (KS) equations:

$$\hat{H} \varphi_i(r) = \varepsilon_i \varphi_i(r) , \quad (2.14)$$

where  $\varepsilon_i$  is the single-electron eigen energy,  $\varphi_i(r)$  is the electron wave function and  $H$  is the Hamiltonian and represented by:

$$\hat{H}(\rho) = T_e + V_{ext} + V_{ee} + V_{XC} , \quad (2.15)$$

such that  $V_{ee}$  represents the electron density interacting with itself (which corresponds to the electron-electron Hartree potential  $V_H$ ) with the format:

$$V_{ee} = \int \frac{\rho(\vec{r}')}{|\vec{r} - \vec{r}'|} d\vec{r}' . \quad (2.16)$$

$V_{ext}$  is the coulomb potential from nuclei affecting the electron gas that exists around it, and  $V_{XC}$  is the exchange-correlation potential which can be found using the relation:

$$V_{XC} = \frac{\partial E_{XC}(\rho)}{\partial \rho} . \quad (2.17)$$

The aim for KS equations to be solved is to find a set of wavefunctions that minimize the energy  $\varepsilon_i$ . [36]

As a result of KS's assumptions, the kinetic energy for the electrons in the Hamiltonian is simply the sum of the single electron kinetic energy. However,  $V_{ee}$  can be confusing due to the fact that we deal with a non-interacting system, and an electron can never interact with itself. These inaccuracies are considered within the exchange-correlation potential terms. The ground state electron density is presented by KS to be:

$$\rho(r) = \sum \varphi_i(\vec{r}) \varphi_i^*(\vec{r}) , \quad (2.18)$$

where  $\varphi_i(\vec{r})$  is the electron wavefunction.

In practice, the KS equations must be solved repeatedly to get consistent results of the electron density. Starting with a guess value for the electron density, let's call it  $\rho_{\text{in}}$ . The Hamiltonian can be constructed since the Hartree and the exchange-correlation potentials depend solely on the electron density. KS equations can be solved and the basis set of wavefunctions can be found. To check if  $\rho_{\text{in}}$  is the actual electron density, the wavefunction set found in the previous step is used to calculate a new electron density  $\rho_{\text{out}}$ . Suppose that the inserted electron density is the same as when we solve the KS equations with the calculated wavefunction set. In this case, it is the actual electron density, and it is called self-consistent. On the other hand, if  $\rho_{\text{out}}$  is not the same as  $\rho_{\text{in}}$ , then  $\rho_{\text{out}}$  is used to redo the process. This method is repeatedly applied until a self-consistent electron density is achieved. This process is summarized in figure (2.1).

In its essence, the exchange-correlation takes into account the quantum mechanical exchange and correlation contributions, corrections for the kinetic energy of the electrons, and corrections for the self-interacting potential resulting from considering the electron density. So far, DFT is in an exact form with no approximations. However, the exchange-correlation term is unknown as an exact formula. Thus, approximated formulas are very essential. The local density approximation (LDA) and the generalized gradient approximation (GGA) are among these approximations

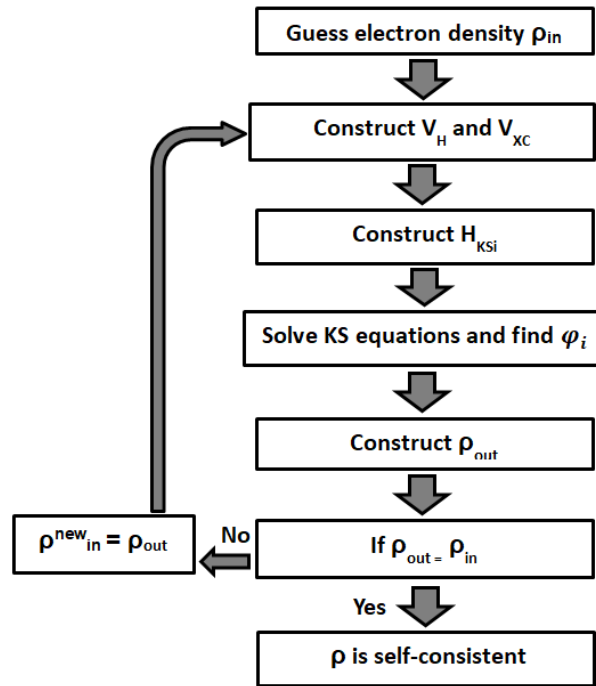


Figure (2.1): Flow chart for the self-consistent field cycles to solve KS equations.

### c) The Local Density Approximation (LDA)

In this approximation, the exchange-correlation energy due to a particular density function could be found by dividing the electron gas into infinitesimal volumes. Each one of these volumes is treated as homogenous electron gas with constant density. Then, the total exchange-correlation energy is the sum of each small volume's contribution: [36]

$$E_{xc}^{LDA} = \int \rho(\vec{r}) \epsilon_{xc}[\rho(\vec{r})] d\vec{r} , \quad (2.19)$$

where  $\epsilon_{xc}[\rho(\vec{r})]$  is the exchange-correlation energy per particle of a uniform electron gas, which solely depends on the electron density  $\rho(\vec{r})$ . The electron density can be divided into two parts: the spin-up electron density and the spin-down electron density [37]. This work deals with the spin-less case.

The exchange-correlation energy per particle is usually separated into two parts:

$$\varepsilon_{xc}[\rho(\vec{r})] = \varepsilon_x[\rho(\vec{r})] + \varepsilon_c[\rho(\vec{r})]. \quad (2.20)$$

Due to Slater, the exchange term is in terms of  $\rho^{1/3}$  [38], making the exchange part much simpler to calculate. The correlation formula is trickier to get and can be calculated numerically [37]. Moreover, one can find tables for the correlation energy calculated numerically for many systems.

LDA has proven to be reasonably accurate in studying many systems such as atoms, molecules, and solids. However, the energy calculations are usually off from the experimental values. [39]

#### **d) The Generalized Gradient Approximation (GGA)**

In reality, the electrons in solid systems are inhomogeneous, unlike the electron gas system, and the electron density fluctuates through space. Therefore, to enhance the accuracy of LDA, the exchange-correlation contribution of every infinitesimal volume is made not only dependent on the local density in that volume but also the density in the neighboring volumes. Mathematically, this can be accomplished by inserting the gradient of the electron density into the formula of the exchange-correlation energy. This is proven to enhance the results for solids. One of the most important approximations that include the gradient within the XC-energy is the Generalized Gradient Approximation (GGA). [40, 41, 42]

Here, the XC-GGA energy correction is given by: [41, 43]

$$E_{XC}^{GGA} = \int d\vec{r} \varepsilon_{XC}[\rho(\vec{r}), \vec{\nabla}\rho(\vec{r})] . \quad (2.21)$$

In this equation, the XC-energy per particle can take different shapes. For example, Perdew in 1986 found the formula of the XC-energy to be: [40]

$$\varepsilon_{XC}[\rho(\vec{r}), \vec{\nabla}\rho(\vec{r})] = \rho^{\frac{4}{3}} [1 + 1.296 s^2 + 14s^4 + 0.2s^6]^{\frac{1}{15}} \quad (2.22)$$

Where  $\rho$  is the electron density, and  $s$  is given by:

$$s = \frac{|\nabla\rho|}{2\rho k_F} \quad (2.23)$$

$$k_F = (3\pi^2\rho)^{\frac{1}{3}} . \quad (2.24)$$

The insertion of the gradient of the electron density can be accomplished in many other ways. One of the good approximations is the Perdew-Burke-Ernzerhof (PBE) approximation, which is going to be used in this work. The PBE XC-energy per particle, given in equation (2.25), is considered a multiple of electron density of a uniform electron gas with a factor  $F_{XC}$ . The factor  $F_{XC}$  depends on the relative spin polarization of the electrons " $\xi$ ",  $s$  with the formula given in equation (2.23), and the local Seitz radius " $r_s$ " which can be found using the relation  $\rho=3/(4\pi r_s^3)$ , where  $\rho$  is the electron density. [43]

$$E_{XC}^{GGA-PBE}[\rho(\vec{r}), \vec{\nabla}\rho(\vec{r})] = \int d\vec{r} \rho(\vec{r}) \varepsilon_X^{Uif}[\rho(\vec{r})] F_{XC}(r_s, \xi, s) . \quad (2.25)$$

**e) Becke-Johnson and the modified Becke-Johnson potentials (mBJ)**

In 2006, Becke and Johnson published their work aiming to enhance the exchange potential values and reduce the error in the energy calculations. The BJ exchange potential is: [44]

$$V_X = V_X^{Slater} + C \sqrt{\frac{\tau}{\rho}}, \quad (2.26)$$

where  $V_X^{Slater}$  is the exchange potential given by Slater [44, 45],  $C$  is a constant:

$$C = \frac{1}{\pi} \sqrt{\frac{5}{12}}, \quad (2.27)$$

and  $\tau$  is the kinetic energy density ( $N$  is the number of electrons):

$$\tau = \frac{1}{2} \sum_i^N |\nabla \psi_i|^2. \quad (2.28)$$

Tran and Blaha, in 2009, performed some modifications to the BJ-exchange potential. The Slater potential was replaced by the Becke-Roussel (BR) [46] which has a similar behavior as the Slater potential. Also, the term containing the kinetic energy density is multiplied by another factor. The mBJ potential is given by equation (2.29). [47]

$$V_X^{mBJ} = aV_X^{BR} + (3C - 2)C \sqrt{\frac{2\tau}{\rho}}. \quad (2.29)$$

The mBJ proved a useful tool to enhance the accuracy of energy calculations, especially the energy band gap values, which play a crucial role in determining the electrical conductivity of solids [47, 48].

## **2.4: Full-potential linearized augmented plane wave method (FP-LAPW)**

As mentioned in subsection (2.3.b), Kohn-Sham equations need to be solved to get consistent results for the electron density. To do that, a basis set of functions are required. From Bloch theorem, the system of electrons in a solid with periodic potential can be described using plane waves (PW). This is a very good approximation in the regions away from the nuclei. However, a huge number of PWs are needed to describe the wave function near the nuclei [35]. Later on, more reliable methods were developed, such as the augmented plane wave method (APW) and the linearized augmented plane wave method (LAPW).

### **a- Augmented plane wave method (APW)**

In 1937, Slater inserted some modifications to the plane wave description of the wavefunction, hence the name “augmented”. This method treats the solid as two regions. Figure 2.2 shows the APW method description of the solids. Region (I) is called the muffin tin spheres (MT), which is represented by non-overlapping spheres, where the potential within them is spherically symmetric and has a similar behavior as a free atom (the potential is inversely proportional to the distance from the nucleus). Each MT sphere is centered at a nuclei position with a radius  $R_{MT}$ . The radius of the muffin spheres is constant for the same type of atoms in the solid. On the other side, region (II) is called the interstitial region, which includes the areas outside the muffin tin spheres and it is assumed to have constant potential. [35, 49]

An essential condition someone needs to keep in mind is that the nearest neighbors' distance in the crystal should always be larger than the sum of the two atoms'  $R_{MT}$ .

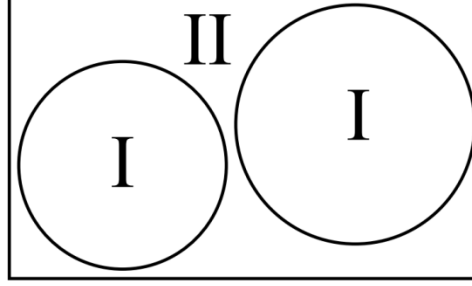


**Figure (2.2): Division of a unit cell into two regions: (I) are muffin-tin regions, and (II) is the interstitial region, for a system of two atoms.**

The electrons' behavior is different in the two regions. For instance, in region (I), the electrons are close to the nuclei and behave like if they were in a free atom. As a result, the electrons in this region can be represented by a multiplication of a radial function and spherical harmonics. However, in region (II), the electrons are far away from the nuclei, the interaction between the interstitial region electrons and the nuclei is negligible. The electrons, therefore, act like they are free. Plane waves can fully describe these electrons. The wavefunction of the electrons in the solids using the APW method is given by equation (2.30).

$$\phi_{\vec{K}+\vec{G}}^{APW}(\vec{r}, \epsilon) = \begin{cases} \frac{1}{\sqrt{V}} \sum_G C_G e^{i(\vec{K}+\vec{G})\cdot\vec{r}} & , r \in \text{II} \\ \sum_{l,m} A_{lm} u_{lm}(\vec{r}, \epsilon) Y_{lm}(\vec{r}) & , r \in \text{I}, \end{cases} \quad (2.30)$$

where  $\phi$  is the wavefunction of the electrons,  $r$  is the position vector,  $V$  is the unit cell volume,  $\vec{G}$  is the reciprocal lattice vector,  $\vec{K}$  is the wave vector of the first Brillouin zone (BZ),  $A_{lm}$  and  $C_G$  are expansion coefficients,  $Y_{lm}$  is

the spherical harmonics, and  $u_{lm}$  is the regular solution to the radial part in the Schrodinger equation of a free atom with energy  $\epsilon$ .

The radial function in equation (2.30) should satisfy the relation (which is extracted by separating the radial part of the wavefunction when substituting it in Schrodinger's equation):

$$-\frac{1}{r^2} \frac{\partial}{\partial r} \left( r^2 \frac{\partial u_{lm}(r)}{\partial r} \right) + \left[ \frac{2m}{\hbar^2} (V(r) - \epsilon_l) + \frac{l(l+1)}{r^2} \right] u_{lm}(r) = 0 . \quad (2.31)$$

One can see that in equation (2.31) if  $V=0$ , the final solution of the wavefunction is plane waves, which is the case of the interstitial region (region (II)). Otherwise, the solution is radial (in the muffin tin spheres: region (I)).

For a realistic description of the electrons in the MT model, the wavefunctions must be continuous at the boundaries of the MT spheres. Applying the boundary conditions gives the formula:

$$u_{lm}(\vec{r}, \epsilon) = \frac{4\pi i^l}{\sqrt{v} u_l(r)} \sum_G C_G J_l(|k + g|) Y_{lm}^*(\vec{K} + \vec{G}) , \quad (2.32)$$

such that  $J_l$  is the Bessel function of order  $l$ .

KS orbitals can be constructed as a linear combination of  $\phi^{APW}$  functions as follows:

$$\varphi_i^{KS} = \sum_j A_j \phi_j^{APW} , \quad (2.33)$$

where  $A_j$  is the expansion coefficient. Here,  $\varphi_i^{KS}$  can be used in solving the KS equations (2.14)

### b- The linearized APW method (LAPW)

The linearized augmented plane wave method (LAPW) scheme was introduced by Andersen in 1975. In this scheme, the radial functions describing the electrons in region (I) are linearized by inserting the first derivative of the radial part of the wavefunction with respect to the energy; thus, the problem is reduced to a linear eigenvalue problem [35, 50, 51].

In LAPW, Taylor expansion is used to represent the radial function of the wavefunction as follows:

$$u_l(r, \epsilon) = u(r, \epsilon_l) + \dot{u}(r, \epsilon_l) + \dots, \quad (2.34)$$

where  $\epsilon_l$  is chosen to be near the expected value of the eigenvalue energy.

The first two terms of the expansion in equation (2.34) were used. Using the new format of the radial part of the wavefunction in region (I),  $u_l(r)$  should satisfy the following relation:

$$\left[ -\frac{\hbar^2}{2m} \frac{\partial^2}{\partial r^2} + \frac{\hbar^2}{2m} \frac{l(l+1)}{r^2} + V(r) - \epsilon_l \right] r u_{lm}(r) = r u_{lm}(r). \quad (2.35)$$

The wavefunction of the electrons using LAPW method is given in equation (2.36).

$$\phi_{\vec{K}}^{LAPW}(\vec{r}, \epsilon) = \begin{cases} \frac{1}{\sqrt{V}} \sum_G C_G e^{i(\vec{K}+\vec{G})\cdot\vec{r}} & , r \in \text{I} \\ \sum_{l,m} [A_{lm} u_{lm}(\vec{r}, \epsilon) + B_{lm} \frac{\partial u_{lm}(\vec{r}, \epsilon)}{\partial \epsilon}] Y_{lm}(\vec{r}) & , r \in \text{II} \end{cases} \quad (2.36)$$

The bases functions describing the electrons and their first derivatives are made continuous at the common boundaries of regions (I) and (II). Applying

the boundary conditions to the boundaries of the MT spheres gives the formulas of  $A_{lm}$  and  $B_{lm}$  as functions of  $(\mathbf{K}+\mathbf{G})$  [35].

LAPW is a more flexible and accurate band structure calculation scheme than APW, since APW uses only the first term in the Taylor expansion in equation (2.34).

The KS orbitals can be achieved the same way as APW using equation (2.33), with the coefficients being determined by the Rayleigh-Ritz variational principle [52].

### **c- Full potential LAPW method (FP-LAPW)**

In APW and LAPW methods, the MT potential is assumed to be spherically symmetric, and the interstitial region has constant potential. The FP-LAPW method gives a more realistic representation of the potential, which leads to more accurate outcomes. The potential is given in equation (2.37) [52].

$$V^{FP-LAPW}(r) = \begin{cases} \sum_{lm} V_{lm}(r) Y_{lm}(\vec{r}) & , r \in I \\ \sum_k V(\vec{k}) e^{i \vec{k} \cdot \vec{r}} & , r \in II \end{cases} , \quad (2.37)$$

where  $\mathbf{k} = \mathbf{K} + \mathbf{G}$ .

In this work, FP-LAPW method is used as a description of the electrons, as well as the GGA approximation of the XC potential. The electronic properties are then enhanced using the mBJ potential.

## Chapter Three

### Lattice structures

Atoms in a solid may be arranged in either symmetric or random fashion. The equilibrium separation distances between the atoms in a solid are fixed at some values to minimize the energy of the system. This can be achieved when the arrangements of the atoms are periodic. [53, 54]

In a crystals, the solid is built from an identical smaller arrangement of atoms, repeated periodically, as shown in figure (3.1). The shapes of these “building blocks” play a role in the material’s properties and they are called the primitive unit cells.

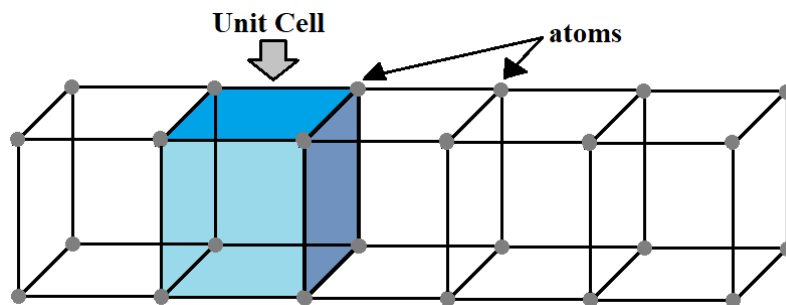


**Figure (3.1): Representation of simple cubic unit cells in a solid with periodic structure.**

To describe any lattice, we need to determine the lattice vectors  $\mathbf{a}$ ,  $\mathbf{b}$  and  $\mathbf{c}$ . So, any point in the lattice can be represented in terms of these lattice vectors as follows:

$$\vec{r}_p = n_1\vec{a} + n_2\vec{b} + n_3\vec{c}, \quad (3.1)$$

where  $n_1$ ,  $n_2$  and  $n_3$  are integers, to indicate the periodic behavior of the lattice.

The values of the lattice vectors are called the lattice constants, and they have the same notations. The angles between the lattice vectors are of great importance in determining the shape of the crystal alongside the lattice constants. The lattice constants  $a$ ,  $b$  and  $c$ , and the angles  $\alpha$ ,  $\beta$  and  $\gamma$  are indicated in figure (3.1).

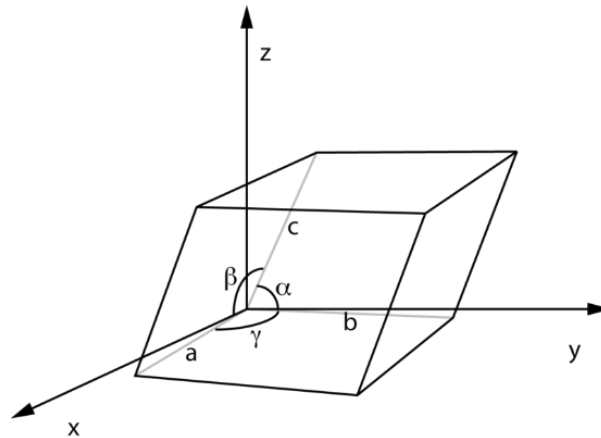


**Figure (3.2): Lattice constants:  $a$ ,  $b$  and  $c$  for a unit cell. The angles between the lattice vectors are:  $\alpha$ ,  $\beta$  and  $\gamma$**

Having different sets of lattice constants and angles changes the lattice structure, and changes the properties of the material drastically. For example, carbon in a graphite structure forms coal with properties such as black color and brittleness. Whereas, if the carbon atoms are arranged in another hexagonal pattern called the diamond structure, diamond is formed with properties such as high strength and shininess.

In this work, five structures of the compounds are considered. These structures are discussed in the following sections [55, 56].

### 3.1: Rocksalt (RS) structure

RS structure is a cubic structure with the space group ( $Fm\bar{3}m-225$ ). In this structure, the atomic positions are  $(0, 0, 0)$  for the first atom and  $(1/2, 1/2, 1/2)$  for the other. The lattice constants for this structure are identical ( $a=b=c$ ). The angles are also identical and equal to  $90^\circ$ .

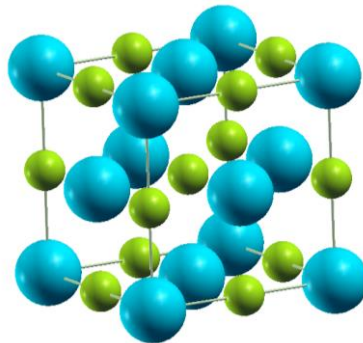


Figure (3.3): Rocksalt structure (RS)

### 3.2: Cesium chloride (CsCl) structure

CsCl structure is also cubic with the same conditions for the lattice constants and the angles as the RS structure. The atomic positions are  $(0, 0, 0)$  for the first atom and  $(1/2, 1/2, 1/2)$  for the second, with a space group ( $Pm\bar{3}m-221$ ).

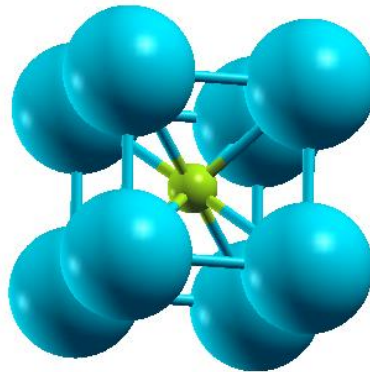


Figure (3.4): Cesium Chloride structure (CsCl)

### 3.3: Zincblende (ZB) structure

The space group for this structure is (F43m-216). It is a cubic structure (same conditions of the lattice constants and angles as the RS structure). The atomic sites are (0, 0, 0) and (1/4, 1/4, 1/4).

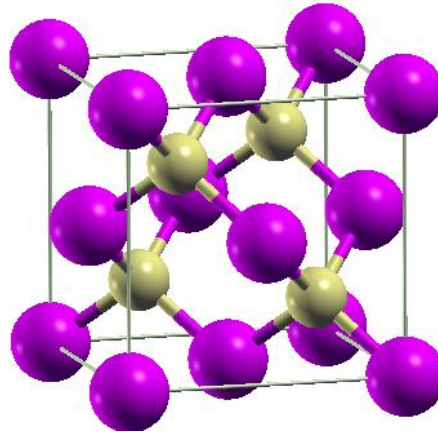
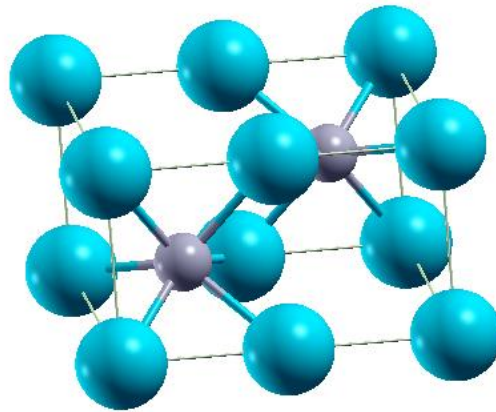


Figure (3.5): Zincblende structure (ZB)

### 3.4: Nickel Arsenide (NiAs) structure

The space group for this structure is (P63mc-194). The atomic positions are (0, 0, 0) and (1/3, 2/3, 1/4). Since this structure is a hexagonal structure, the lattice constants are not all the same; a and b are equal while the lattice constant c has different value. Moreover, the angle  $\gamma = 120^\circ$ , while  $\alpha$  and  $\beta$  equal  $90^\circ$ . The symmetry in hexagonal structures does not exist as much as in the cubic structures. As a result, more parameters are usually addressed when studying the hexagonal structures.



**Figure (3.6):** Nickel arsenide structure (NiAs)

### **3.5: Wurtzite (WZ) structure**

WZ is a hexagonal structure with a lattice group of (P63mc-186). The atomic sites are  $(1/3, 2/3, 0)$  and  $(1/3, 2/3, u)$ , where  $u$  is an internal parameter that depends on the lattice constants and the type of atoms within the crystal. The lattice parameters and the angles have the same conditions as NiAs structure.

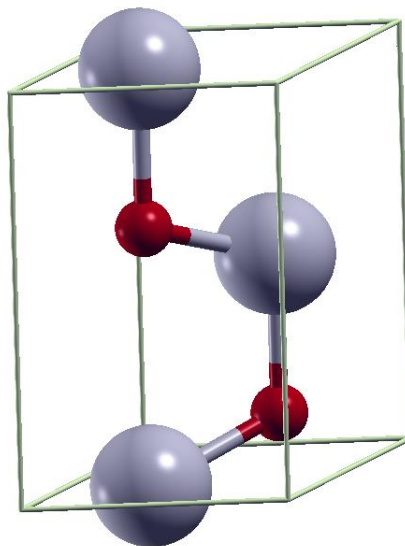


**Figure (3.7):** Wurtzite structure (WZ)

## Chapter Four

### Methodology

The practical tools needed to study the compounds KI and RbI are presented in this chapter. The WIEN2k software package used for this work is addressed. Also, the methodology of calculating the structural properties for both cubic and hexagonal structures is displayed, as well as the method of calculating the pressure at which the compounds go through phase transformation. Moreover, the needed tools to address the electronic and the elastic properties are presented, with the methodologies of calculating the elastic moduli and testing the stability of the compounds in any structure.

#### 4.1: WIEN2k software package

The WIEN2k package is a program written in Fortran 90. It was developed by Peter Blaha, Karlheinz Schwarz, and others, from the Institute of Materials Chemistry of the Vienna University of Technology [57]. The first public release of the code was in 1990, and the code is being developed continuously. This program is relatively of low cost and fast performance.

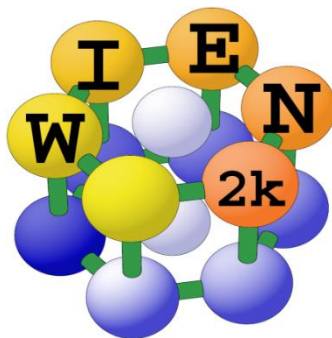


**Figure (4.1):** WIEN2k software package logo

WIEN2k uses density functional theory (DFT) as a framework to obtain results concerning compounds' properties including structural, electronic and elastic properties. Kohn Sham equations of density functional theory are being solved using the full-potential linearized augmented plane wave (FP-LAPW) basis set. Considering the potential of the electrons' system, WIEN2k allows the user to choose from different potential approximations such as LDA and GGA. Also, many GGA approximations are available, such as the PBE approximation [57].

#### **4.2: Structural properties**

Describing the structure of a compound requires the search for the dimensions of the lattice that make it the most stable, as well as the behavior of the crystal under mechanical stress. The structural properties can be calculated as follows:

##### **a- Murnaghan's equation of state**

Murnaghan's EOS has many forms and it connects the energy, volume, pressure and Bulk modulus in one equation. The format of Murnaghan's equation used in this work is: [58]

$$E(V) = E_0 + \frac{BV}{\dot{B}} \left[ \left( \frac{V_0}{V} \right)^{\dot{B}} \frac{1}{\dot{B}-1} + 1 \right] - \frac{BV_0}{\dot{B}-1}, \quad (4.1)$$

where  $E$  is the energy,  $E_0$  is the minimum energy,  $B$  is the Bulk modulus at the equilibrium volume,  $\dot{B}$  is the first derivative of Bulk modulus (with respect to pressure),  $V$  is the volume,  $V_0$  is the equilibrium volume, and  $P$  is the pressure (given by  $P = -dE/dV$ ).

In WIEN2k, the energy values are calculated for some chosen volume values, and then the values of both volumes and energies are fitted into Murnaghan's equation to find the other parameters.

### **b- The Bulk modulus**

The bulk modulus, indicated by the symbol `B`, describes the behavior of the lattice under pressure. The higher the value of the Bulk modulus of a material, the more it can resist an external pressure (lower change in the volume) [59]. Bulk modulus, measured in Pascal, is given by the following relation:

$$B = -V \frac{dP}{dV} = V \frac{d^2E}{d^2V} . \quad (4.2)$$

The following subsections present the detailed process of calculating the structural parameters for the compounds KI and RbI in the whole studied structures in this thesis.

#### **4.2.1: Structural properties for cubic structures**

As mentioned in chapter 3, the lattice structure can be described by lattice parameters a, b and c. The methodology used to find these parameters for the cubic structures: RS, CsCl and ZB structures, is as follows:

- 1- A guess value of the lattice constant is used to initialize the compound and perform SCF cycles.

- 2- The optimization calculation is held at constant ratio of a, b and c. Many values for the volume of the lattice are considered. The energy is numerically calculated by WIEN2k for each volume value included in this step.
- 3- The results from the previous step are fitted into Murnaghan's equation of state [58], which gives the needed structural parameters. The results include the optimized lattice constant a, the bulk modulus, the first derivative of the bulk modulus with respect to the pressure, the volume at which the lattice is at the lowest energy, and the minimum energy value, in addition to the chart of energy versus volume.

#### **4.2.2: Structural properties for NiAs structure**

For the NiAs structure, the steps to study structural parameters are as follows:

- 1- Guess values of the lattice constants are used to initialize the compound and perform SCF cycles. Optimization calculations are held for the c/a ratio at constant volume. The volume can be calculated using the following relation:

$$V = \frac{\sqrt{3}}{2} \left(\frac{c}{a}\right) a^3 . \quad (4.3)$$

- 2- The calculation results give an optimized value of the ratio c/a, which is the value of c/a that minimizes the energy. The optimized c/a can be applied to equation (4.3) to calculate the optimized lattice parameter a, then c accordingly.

- 3- . Optimization of the volume at a constant ratio of the lattice parameters is held for the new optimized values of the parameters, which gives the structural properties using Murnaghan's EOS.

#### **4.2.3: Structural properties for WZ structure**

As for the WZ structures, it is more complicated since the WZ structure includes an additional parameter to optimize ( $u$ ) (as mentioned in chapter 3).

The methodology is as follows:

- 1- The same steps done for the NiAs structure are used in the WZ structure to obtain the optimized values of the lattice parameters. With an additional guess value of  $u$  in the first step.
- 2- Initialization and SCF cycles are held for the optimized lattice parameters and the guess value of the parameter  $u$ . The minimum energy value is registered for this step.
- 3- Initialization and SCF cycles are performed to the same lattice constants with a slight variation of the parameter  $u$ . The energy value associated with the input parameters is registered.
- 4- The registered energy values are compared. The least value of the minimum energy is associated with the closer value of  $u$  to the best optimization of  $u$ .
- 5- The previous two steps are repeated to get the needed accuracy of  $u$  value.
- 6- Initialization and SCF cycles are applied to the optimized parameters (including the optimized value of  $u$ ). Volume optimization is applied at

constant  $a$ ,  $b$  and  $c$  ratio, and the graph  $E$  vs.  $V$  is achieved and fitted into Murnaghan's EOS to get the structural parameters.

#### 4.2.4: Phase transformation and transition pressure

Phase transformation means a change in the lattice structure, which leads to a change in the properties. Experiments have shown that subjecting a material to high pressures can cause an observable change in its properties indicating changes on the structures [5, 18, 12, 60]. For example, many experiments have shown that applying high pressure into KI changes the lattice structure from RS to CsCl, see figure (4.2).

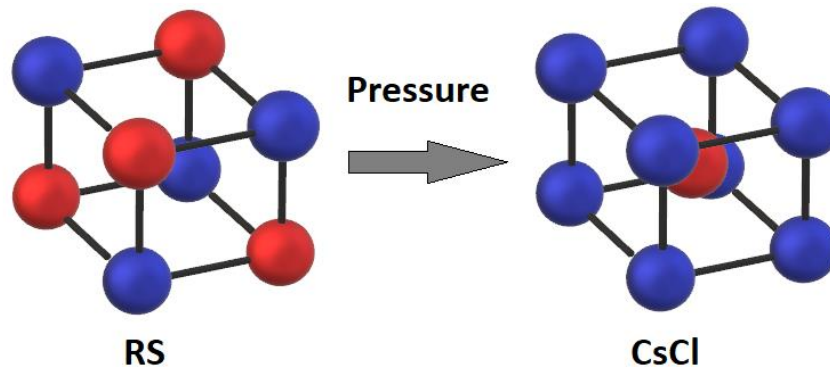


**Figure (4.2): High pressure effect on lattice structure of KI.**

In order to calculate the pressure at which a phase transformation occurs, EOS graphs are usually used. The pressure for any point in the EOS graph for a material's structure is calculated as the slope of the tangent at that point, as shown in figure (4.3).

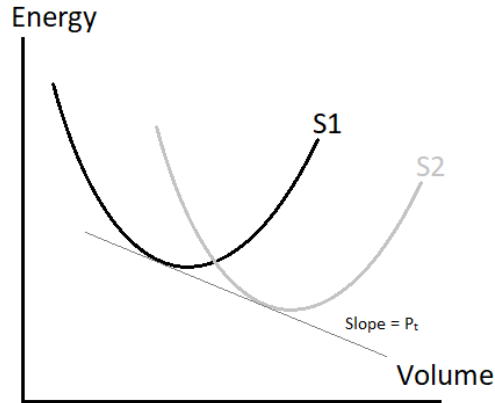


**Figure (4.3): Extracting the transition pressure (between the structures S1 and S2) from EOS graphs.**

For a graph containing two structures for a material, the slope of the common tangent for both curves gives the pressure at which a phase transformation occurs between these two structures. This is provided by the formula:

$$P_t = - \frac{dE}{dV} , \quad (4.4)$$

where  $P_t$  is the transition pressure,  $E$  is the energy, and  $V$  is the volume. Regarding the sign, a positive value of the transition pressure represents a compression process to get the transformation. On the other hand, a negative sign of the pressure represents an expansion process.

A more accessible and more accurate method of calculating the transition pressure is to use the enthalpy  $H$ , which has the formula: [61]

$$H = E + P * V, \quad (4.5)$$

The enthalpy for two structures will be identical at the point of transformation. This can be proven starting from equation (4.4) as follows:

$$P_t = -\frac{dE}{dV},$$

$$P_t dV = -dE,$$

By integrating both sides:

$$P_t(V_2 - V_1) = -(E_2 - E_1),$$

Rearranging the variables:

$$E_1 + P_t V_1 = E_2 + P_t V_2, \quad (4.6)$$

Using equation (4.5):

$$H_1 = H_2. \quad (4.7)$$

Practically, having a graph of enthalpy vs. pressure for two structures that go through transition will have a crossing point, since both coordinates are the same at the phase transformation (both enthalpy and pressure). The pressure at this point is the transition pressure. See figure (4.4)

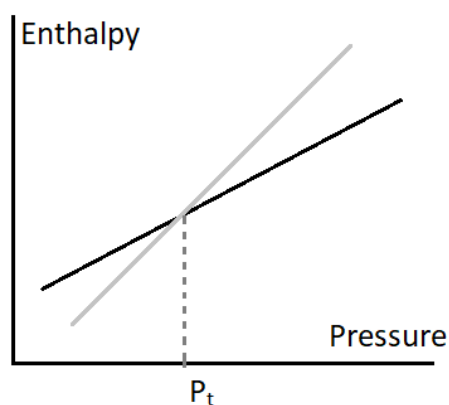


**Figure (4.4): Calculating transition pressure using the enthalpy.**

### **4.3: Electronic properties**

The electronic properties describe the state and behavior of the electrons in the studied compounds. They can be introduced using certain parameters and representations as follows:

#### **4.3.1: Band structure**

Each lattice has an associated reciprocal lattice in k-space, with the special primitive cell called the first Brillouin zone (BZ). Each type of the crystal is associated with a specific shape of the BZ. For example, in figure (4.5), the 1<sup>st</sup> BZ for an FCC lattice is shown.

To study the energy density for each point in the BZ, symmetry can be used to simplify the results. Some regions in the BZ are repeated within it. The minimum number of points representing all the regions in the BZ is used to calculate the bands' energy, including the energy throughout the lines connecting these high symmetry points. In the results, a band structure graph will have the energy density on the y-axis, and the high symmetry k-points' path on the x-axis.

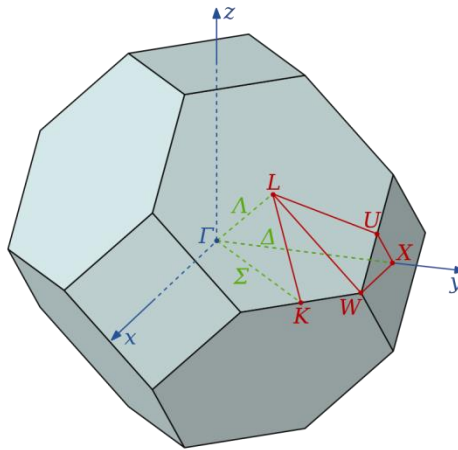


**Figure (4.5): First brillouin zone for FCC lattice.**

### 4.3.2: Electron density of state (DOS)

The density of states can be defined as the number of energy levels available for a given energy. The total DOS is a combination of each orbital's contribution to the number of states for an energy value. In this work, the total DOS for the compounds is presented, as well as each atom's DOS and the orbitals contributions of both atoms in the compounds.

For semiconductors and insulators, the DOS has a gap between the conduction and valence bands with zero value for DOS, representing the energy band gap.

### 4.3.3: Energy band gap

According to band theory, a material with a periodic structure has an energy distribution over bands instead of a single atom or a single compound's discrete form of the energy levels. An energy band is called the valence band; it is filled with electrons at low temperatures and usually exists below the

Fermi level. On the other hand, the conduction bands are occupied when temperature is raised, they typically exist above the Fermi energy, and their occupancy depends on the type of the material and contributes to the material's conductivity.

The energy band gap  $E_g$  is calculated by WIEN2k using the approximation GGA-PBE, which underestimates the energy gap values. Therefore, mBJ is implied to enhance the results.  $E_g$  is calculated as the difference between the maximum valence band (MVB) energy and the minimum conduction band (MCB) energy.

#### **4.4: Elastic properties**

Elastic properties are related to the response of the crystal when an external force is applied to it. Elastic behavior is represented in many parameters such as the elastic constants, Bulk, Shear and Young moduli.

##### **4.4.1: Stress, strain and elastic constants**

Stress, represented as  $\sigma$ , is a tensor that describes force distribution on a surface .Stress tensor consists of linear stress terms (diagonal terms) and shear stress terms (non-diagonal terms):

$$\sigma = \begin{bmatrix} \sigma_{11} & \sigma_{12} & \sigma_{13} \\ \sigma_{21} & \sigma_{22} & \sigma_{23} \\ \sigma_{31} & \sigma_{32} & \sigma_{33} \end{bmatrix} . \quad (4.8)$$

Strain also consists of two types of terms, normal strain terms that describe the length rate of change of the stressed body in a specific direction, and

shear strain terms that measure the distortion of the stressed body. [62] Stress and strain are related with the following relation [63]:

$$\left[ \frac{\partial \sigma_{ij}(I)}{\partial \epsilon_{kl}} \right]_F = C_{ijkl} + \frac{1}{2} [\sigma_{il}(F)\delta_{jk} + \sigma_{jl}(F)\delta_{ik} + \sigma_{ik}(F)\delta_{jl} + \sigma_{jk}(F)\delta_{il}] - \sigma_{ij}(F)\delta_{kl}, \quad (4.9)$$

where  $\sigma_{xy}$  are the stress tensor components (x and y could be  $i, j, k$  or  $l$ ),  $\epsilon_{kl}$  are the strain's tensor components,  $\delta_{xy}$  are delta functions ( $\delta_{xy}=1$  if  $x=y$ , 0 otherwise), and  $C_{ijkl}$  are the elastic constants that depend on the structure and type of the material and play a vital role in determining the elastic properties of the material.

With  $i, j, k$  and  $l$  having values from 1 to 3, there are a considerable number of 81 elastic constants! However, thanks to symmetry, they can be reduced into 21 constants in general. For cubic structures, the number of elastic constants can be reduced even further due to the high symmetry; only three independent constants ( $C_{11}$ ,  $C_{12}$  and  $C_{44}$ ) are needed. [64]

In hexagonal structures, symmetry is less present than in cubic structures; this requires more elastic constants to study the elastic properties. The elastic constants in hexagonal structures are:  $C_{11}$ ,  $C_{12}$ ,  $C_{13}$ ,  $C_{33}$  and  $C_{55}$ . [65]

Elastic constants can be found experimentally and can be calculated using theoretical approximations, as in this work.

#### 4.4.2: Stability conditions

One of the many benefits of knowing the elastic constants is to examine the stability of the material. For the cubic structures, the elastic constants must satisfy the Born stability criteria to be considered stable solids [66], as follows:

$$C_{11} - C_{12} > 0, \quad C_{44} > 0 \quad \text{and} \quad C_{11} + 2C_{12} > 0. \quad (4.10)$$

For the hexagonal structure, the previous conditions must be satisfied as well as additional conditions required for stability: [67]

$$C_{11} > |C_{12}| \quad \text{and} \quad C_{55} > 0, \quad (4.11)$$

where  $C_{44} = C_{55}$  in hexagonal structures.

#### 4.4.3: Elastic moduli

Voigt and Reuss are schemes of approximations to find the elastic and mechanical properties. The Hill's approximation gives the average of the Voigt and Reuss approximations [68, 69, 70].

Many factors are available to be used in describing the elastic and mechanical properties of materials. The following moduli, factors, or ratios are of great importance for this study:

##### a) Bulk modulus (**B**)

The bulk modulus of cubic crystals has the same formula using Voigt [68], Reuss [69] or Hill's [70] methods and it can be calculated in terms of the elastic constants as follows: [71]

$$B^{Cubic} = \frac{C_{11}+2C_{12}}{3} . \quad (4.12)$$

Also, at zero temperature, the bulk modulus has the formula: [72]

$$B = -V \frac{dP}{dV} = V \frac{d^2E}{dV^2} , \quad (4.13)$$

where P is the pressure, E is the total energy, and V is the volume of the unit cell.

For the hexagonal structure, the Bulk modulus (B) formula found by Voigt is given in terms of elastic constants by the relation: [68, 73, 74]

$$B_V^{Hex} = \frac{1}{9}(2C_{11} + C_{33} + 2C_{12} + 4C_{13}) . \quad (4.14)$$

The bulk modulus found by Reuss for the hexagonal structures has the following formula: [69, 73]

$$B_R^{Hex} = \frac{(C_{11}+C_{12})C_{33}-2C_{13}^2}{C_{11}+C_{12}+2C_{33}-4C_{13}} . \quad (4.15)$$

While Hill's bulk modulus for the hexagonal structures is given as the average of Voigt and Reuss formulas: [70, 73]

$$B_H^{Hex} = \frac{B_V+B_R}{2} . \quad (4.16)$$

### b) Shear modulus (S)

The shear modulus (S) considers the behavior of a material under shear strain, and it has several formulas [59]. The Voigt, Reuss, and Hill's formulas for cubic structures are given in equations (4.17), (4.18) and (4.19), respectively [75]

$$S_V^{Cubic} = \frac{C_{11} - C_{12} + 3C_{44}}{5}, \quad (4.17)$$

$$S_R^{Cubic} = \frac{5(C_{11} - C_{12})C_{44}}{3(C_{11} - C_{12}) + 4C_{44}}, \text{ and} \quad (4.18)$$

$$S_H^{Cubic} = \frac{S_V^{Cubic} + S_R^{Cubic}}{2}. \quad (4.19)$$

In hexagonal structures, the shear modulus has different formulas, the Voigt, Reuss and Hill's formulas are shown in equations (4.20), (4.21) and (4.22), respectively. [68, 69, 70, 76]

$$S_V^{Hex} = \frac{1}{30} [7C_{11} - 5C_{12} + 12C_{44} + 2C_{33} - 4C_{13}], \quad (4.20)$$

$$S_R^{Hex} = \frac{5}{2} \left[ \frac{WC_{44}C_{66}}{3B_V^{Hex}C_{44}C_{66} + W(C_{44} + C_{66})} \right], \text{ and} \quad (4.21)$$

$$S_H^{Hex} = \frac{S_V^{Hex} + S_R^{Hex}}{2}, \quad (4.22)$$

where W in equation (4.21) stands for:

$$W = (C_{11} + C_{12})C_{33} - 2C_{12}^2, \quad (4.23)$$

And  $C_{66}$  is given as: [74]

$$C_{66} = \frac{1}{2}(C_{11} - C_{12}) . \quad (4.24)$$

**c) The bulk to shear (B/S) ratio**

The ratio B/S was found to give information about the brittleness of a material. According to Pugh, for  $B/S < 1.75$  indicates a brittle behavior of the material. Otherwise, the material is considered ductile. [77]

**d) Hardness (H)**

Another factor can be deduced from the bulk and shear moduli, which is the hardness of a material (H). H describes a material's resistance to volume changes. Vickers hardness is considered a good description of the material's resistance to changing the volume. The formula of Vickers hardness proposed by Chen is: [78]:

$$H_v = 2 \left( \frac{S^3}{B^2} \right)^{0.585} - 3 . \quad (4.25)$$

**e) Young modulus (Y)**

Young's modulus (Y) is given in terms of the bulk and shear moduli for all types of structures [75]:

$$Y = \frac{9 S B}{S+3B} . \quad (4.26)$$

In equation (4.26), the higher the value of  $Y$ , the stiffer the material is [79].

### f) Poisson's ratio ( $\nu$ )

According to Koval, Poisson's ratio can be defined as "the ratio of the relative contraction strain normal to the applied force to the relative extension strain in the direction of the applied force" [80]. This definition is summarized in figure (4.6)

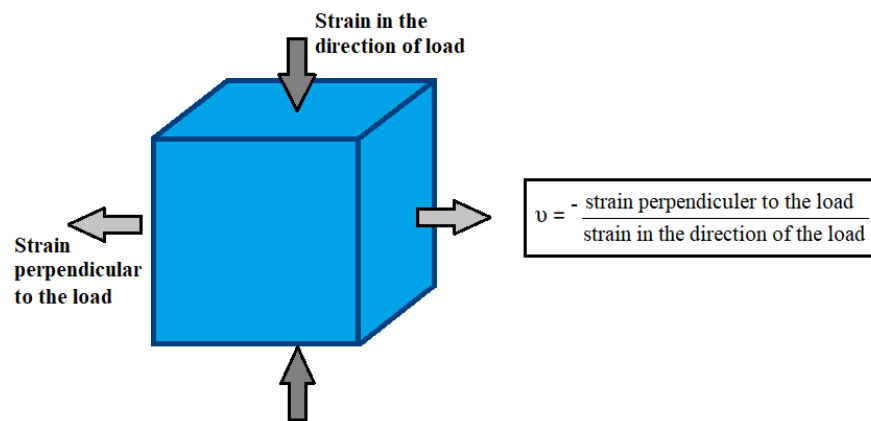


**Figure (4.6): Poisson's ratio in terms of strain**

Also,  $\nu$  can be represented in terms of bulk and shear moduli as follows:

$$\nu = \frac{3B - 2S}{2(3B + S)} \quad (4.27)$$

Poisson's ratio is very beneficial in checking the type of bonding within the crystal. Values of higher than 0.25 are related to ionic bonding, while values lower than 0.25 denote that the type of bonding is covalent [79].

### g) The anisotropic factor (A)

The atomic arrangements of the material in different directions are taken into consideration via the elastic anisotropic factor (A) [81]. Also, A is an important tool to predict the hardness of a material [82].

A is given for the cubic and hexagonal structures in the formulas (4.28) and (4.29).

$$A_{Cubic} = \frac{2C_{44}}{C_{11}-C_{12}} , \text{ and} \quad (4.28)$$

$$A_{Hex} = \frac{4C_{44}}{C_{11}+C_{33}-2C_{13}} . \quad (4.29)$$

If a material has an isotropic factor of 1, it is considered as a completely isotropic material, while values higher or lower than 1 describe the elastic anisotropy of the material. [82, 83]

$$A = \begin{cases} 1 , & \textit{Isotropic material} \\ \textit{otherwise}, & \textit{Anisotropic material} . \end{cases} \quad (4.30)$$

#### **h) The Cauchy pressure (Cs)**

An essential tool that gives information about the nature of the bonds between the atoms within the lattice is the Cauchy pressure  $C_s$  given as:

$$C_s^{Cubic} = C_{12} - C_{44} , \text{ and} \quad (4.31)$$

$$C_s^{Hex} = C_{12} - C_{55} . \quad (4.32)$$

A negative value of Cauchy's pressure indicates the dominance of covalent bonding within the lattice; otherwise, ionic bonding dominates within the material [84].

## Chapter Five

### Results and analysis

The obtained results in this work are presented within this chapter. These results describe the structural, electronic and elastic properties for KI and RbI compounds in RS, CsCl, ZB, NiAs and WZ structures.

#### 5.1: Potassium iodide (KI) compound

##### 5.1.1: Structural properties

Structural parameters are obtained by fitting the calculated energies at each volume around the equilibrium volume to Murnaghan's equation of state [58]. The calculated parameters are the lattice parameter ( $a$ ), bulk modulus ( $B$ ), and the first pressure derivative of the bulk modulus ( $\dot{B}$ ) for the cubic structures (RS, CsCl and ZB), with the additional lattice parameters  $c$  and  $u$  for the hexagonal structures (NiAs and WZ). The equilibrium volume is also found as well as its associated minimum energy. The calculated structural properties are listed in table (5.1.1) for the cubic structures in addition to the available previous experimental and theoretical work, and table (5.1.2) for the hexagonal structures.

The calculated RS structural parameters are in good agreement with other experimental and theoretical results listed in table (5.1.1).

The equation of states for KI with RS, CsCl, ZB, NiAs and WZ structures are shown in figure (5.1.1). From this figure, the absolute minimum energy is associated with the RS structure, which indicates that the ground state for the compound KI is the RS structure.

**Table (5.1.1): The structural properties of KI in RS, CsCl and ZB structures with other available experimental and theoretical results.**

KI	a(opt) (Å <sup>0</sup> )			B(GPa)		B	V <sub>0</sub> (a.u. <sup>3</sup> )	E <sub>0</sub> (Ry)
	Structure	This work	Exp. results	Theo. work	This work			
<b>RS</b>	7.1877	7.067 <sup>[a]</sup>	7.065 <sup>[b]</sup> 7.03 <sup>[c]</sup> 7.213 <sup>[d]</sup> 7.094 <sup>[e]</sup>	10.36	11.6 <sup>[a]</sup> 13.8 <sup>[c]</sup>	4.3265	626.4918	-15442.447956
<b>CsCl</b>	4.3427	-	-	12.2606	-	5.1195	552.6732	-15442.437593
<b>ZB</b>	7.9994	-	-	6.9266	-	4.3277	863.5860	-15442.434566

aRef. [13], bRef. [88], cRef. [14], dRef. [23], eRef. [7]

**Table (5.1.2): The structural properties of KI in NiAs and WZ structures**

KI	NiAs	WZ
Structure		
a=b(opt) ( $\text{\AA}^0$ )	5.511947	6.056759
c(opt) ( $\text{\AA}^0$ )	9.479446	7.850772
c/a(opt)	1.7198	1.2962
u(opt)	-	0.483
B(GPa)	10.0956	7.5095
$\dot{B}$	5.1908	4.3707
$V_0(\text{a.u.}^3)/2\text{atoms}$	627.4722	790.92715
$E_0(\text{Ry})/2\text{atoms}$	-15442.433147	-15442.439108

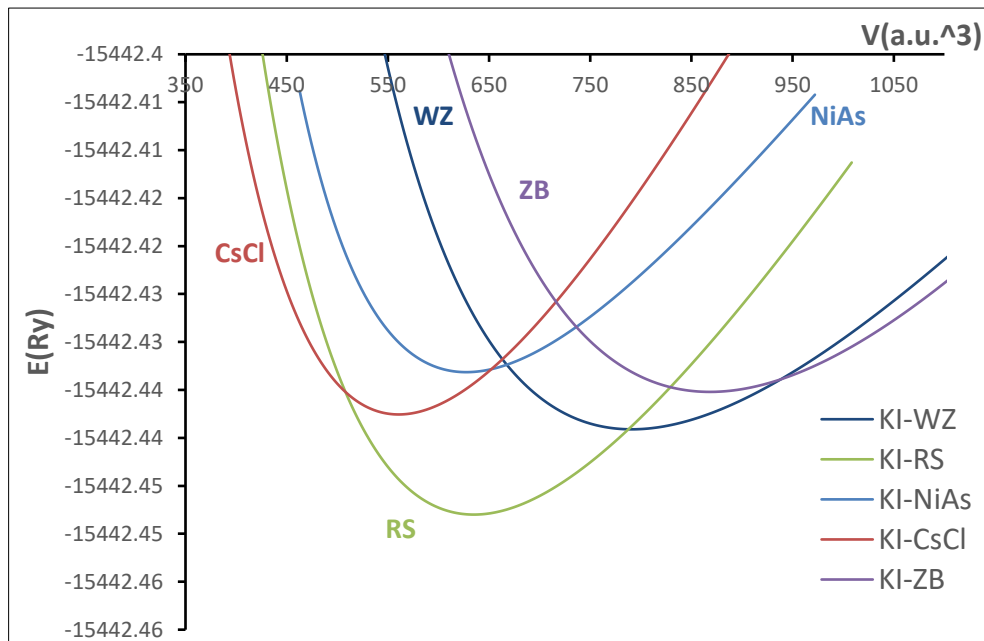


**Figure (5.1.1): Energy (in Ry) calculated at each volume versus the volume (in  $\text{a.u.}^3$ ) for KI in RS, CsCl, ZB, NiAs and WZ structures**

### 5.1.2: Phase transformations

KI can transform into other structures than RS by controlling the pressure upon the sample. The transformation from RS to CsCl requires a compression process that is associated with a positive transition pressure

value. On the other hand, other transformations such as RS to ZB and RS to WZ require an expansion process associated with a negative transition pressure.

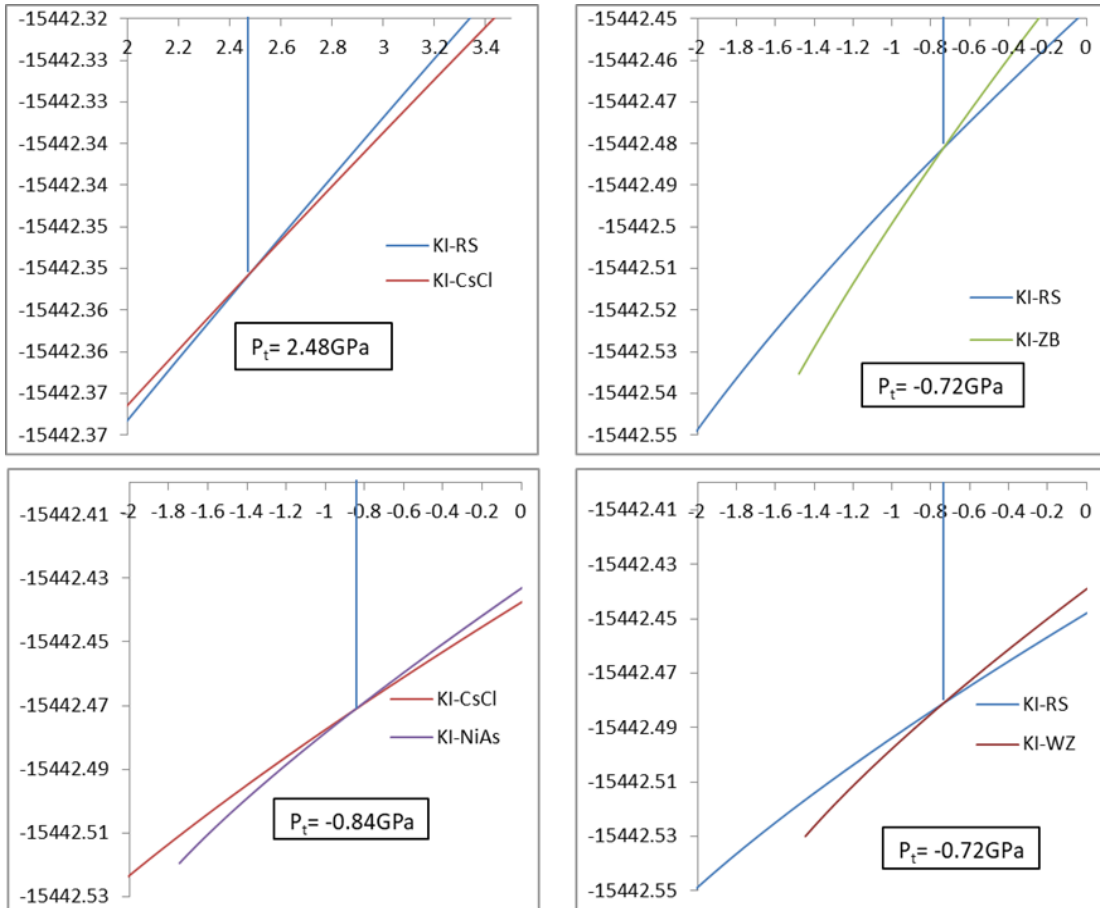


**Figure (5.1.2): Enthalpy  $H$  (in Ry) versus pressure  $P$  (in GPa) for KI phase transformations using PBE-GGA approximation**

The enthalpy versus pressure graphs are shown in figure (5.1.2), which was used to obtain the transition pressures. The values of the transition pressures are listed in table (5.1.3) as well as some of the available experimental and calculated results. The values of  $P_t$  obtained in this work are consistent with the other studies mentioned in table (5.1.3).

**Table (5.1.3): Transition pressures for the transition of KI between various structures along other available experimental and theoretical results.**

KI	RS→CsCl			CsCl→NiAs	RS→ZB	RS→WZ
	This work	Experimental work	Other theoretical results			
Transition pressure	This work	Experimental work	Other theoretical results	This work	This work	This work
Pt (GPa)	2.48	1.73 <sup>[b]</sup> 1.9 <sup>[c]</sup>	2 <sup>[a]</sup>	-0.84	-0.72	-0.72

<sup>a</sup>Ref. [7], <sup>b</sup>Ref. [17], <sup>c</sup>Ref. [5]

### 5.1.3: Electronic properties

The band structure (BS) was attained using the PBE-GGA and mBJ-GGA approximations, and the energy is calculated along high symmetry lines. Calculations were done with the optimized lattice constants. The BS graphs are presented in figure (5.1.3) for KI in each of the examined structures.

The band gap between the valence and the conduction bands can be seen in the BS graphs.  $E_g$  is calculated as the difference between (MVB) and (MCB) using both: mBJ and GGA approximations and the values are listed in table (5.1.4) along with previous studies' results for the RS structure. The GGA approximation underestimates the value of energy band gap. Meanwhile, the results of the mBJ are in good agreement with the other available experimental and theoretical outputs. For the structures: RS, ZB, NiAs and WZ, direct energy band gaps along  $\Gamma$  symmetry point are observed with the values given in table (5.1.4). However, the band gap in CsCl structure is an indirect band gap between  $\Gamma$  and M high symmetry points.

The energy band gap values indicate that KI is a semiconductor in all the structures considered in this thesis: RS, CsCl, ZB, NiAs and WZ. The energy separation between the conduction and valence states was chosen to be -10 Ry. Therefore, the core states for the potassium are 1s and 1p, while the states from 3s up to 4s are considered valence states. For the iodide, the core states are from 1s to 4s, and the valence states are from 4p to 5p. This applies for all the included structures of KI in this thesis.

The DOS shows the number of states that can be occupied by electrons as a function of the energy. The DOS graphs for KI are shown in figures (5.1.4), (5.1.5), (5.1.6), (5.1.7) and (5.1.8). In the DOS graphs, the dotted line represents the Fermi energy ( $E_F$ ). For the energies below the Fermi energy in the structures RS, CsCl, ZB and NiAs, one peak takes place. The main contribution to the DOS is made by the p-state in the iodide, with a small contribution from the p-state in the potassium. Whereas, in the WZ structure, three peaks can be seen; the s-state in the potassium contributes with the first peak, the second peak is a combination of two contributions: p-state in potassium and s-state in the iodide, and the third peak is made by the p-state in the iodide with a small contribution from the p-state in the potassium.

On the other hand, the DOS for the energies above  $E_F$  has continuous peaks made mainly by the potassium, with compatible contributions from its s and p states, in addition to a small contribution from the iodide, mainly by the d states.

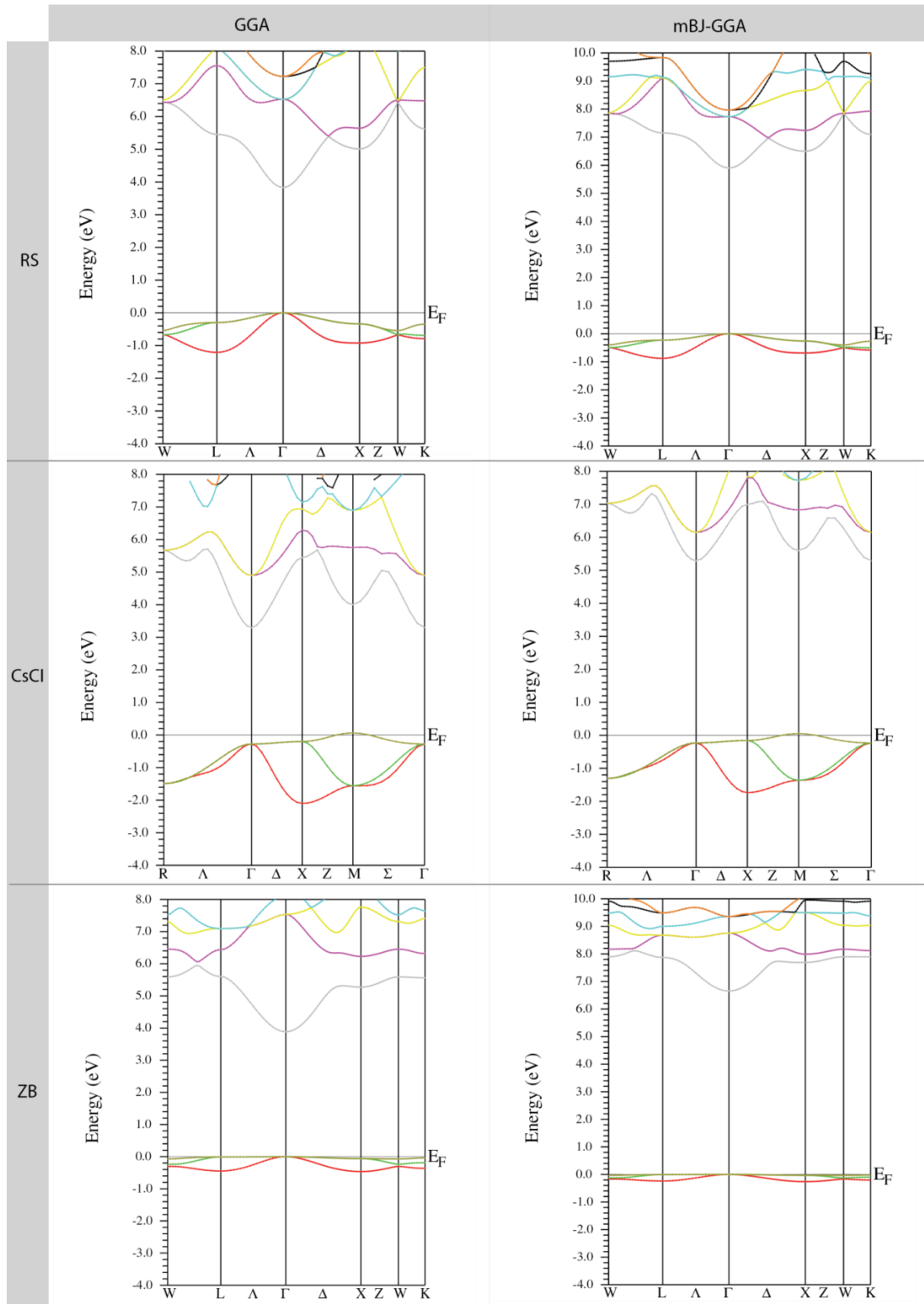


**Figure (5.1.3.a): Band structure for KI in the cubic structures RS, CsCl and ZB using the approximation GGA and mBJ.**

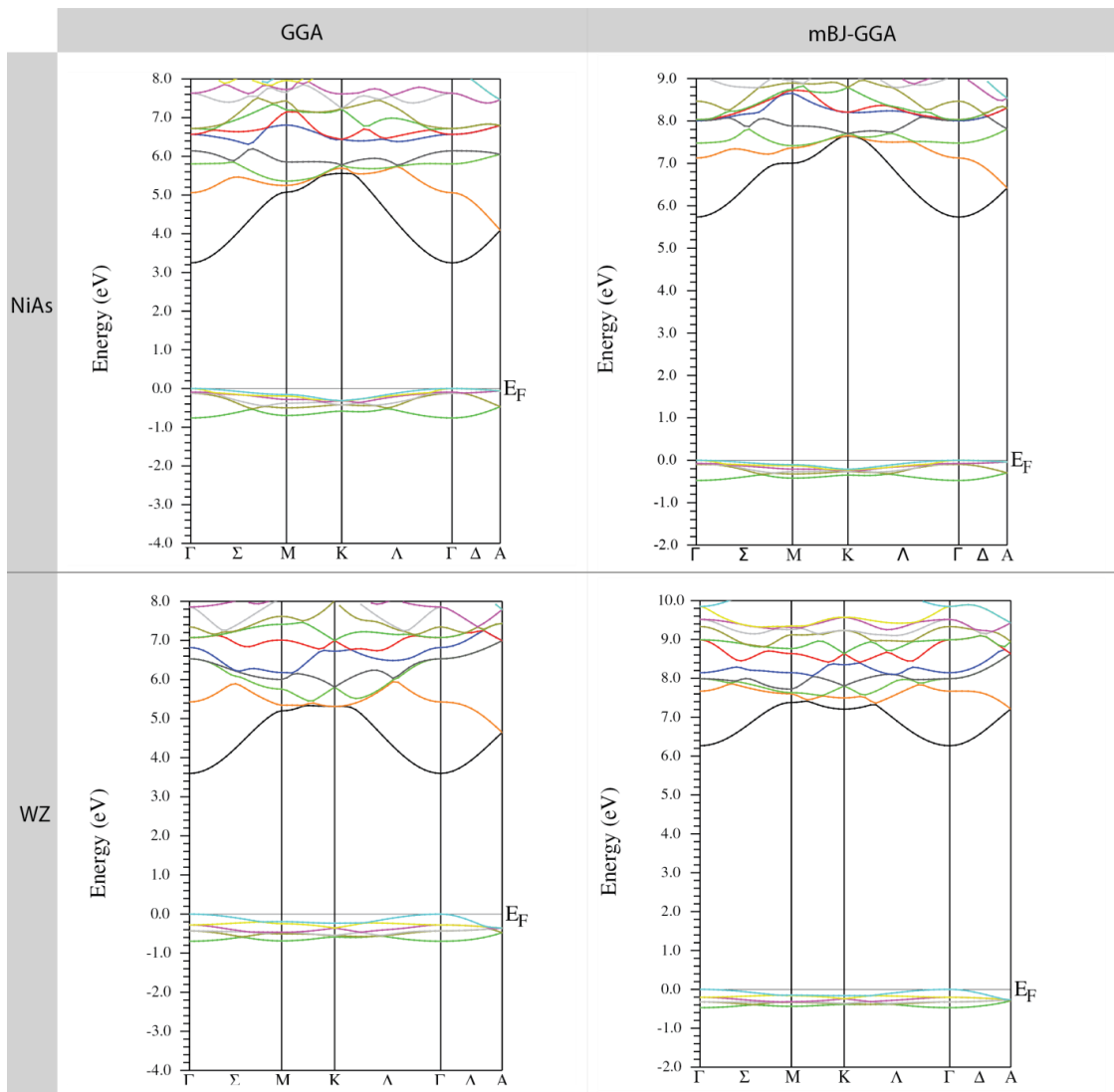


**Figure (5.1.3.b): Band structure for KI in the hexagonal structures NiAs and WZ using the approximation GGA and mBJ.**

**Table (5.1.4): Energy band gap (in eV) for KI in the examined structures, using the approximations GGA and mBJ, with other available experimental and theoretical results.**

KI											
RS			CsCl		ZB		NiAs		WZ		
This work		Exp. Results	Other theoretical Work		This work		This work		This work		
GGA	mBJ		GGA	mBJ	GGA	mBJ	GGA	mBJ	GGA	mBJ	
3.83 3	5.902	6.34 <sup>[a]</sup>	5.984 <sup>[b]</sup> , 6.2 <sup>[c]</sup> , 4.26 <sup>[d]</sup> , 5.951 <sup>[e]</sup> <sub>mBJ</sub>	3.492	5.442	3.884	6.653	3.246	5.73 2	3.597	6.264

aRef. [21], bRef. [7], cRef. [85], dRef. [22], eRef. [23]

In the total DOS graph, the flattened line with zero DOS represents the forbidden area with the energy band gap, which separated the valence from the conduction electrons.

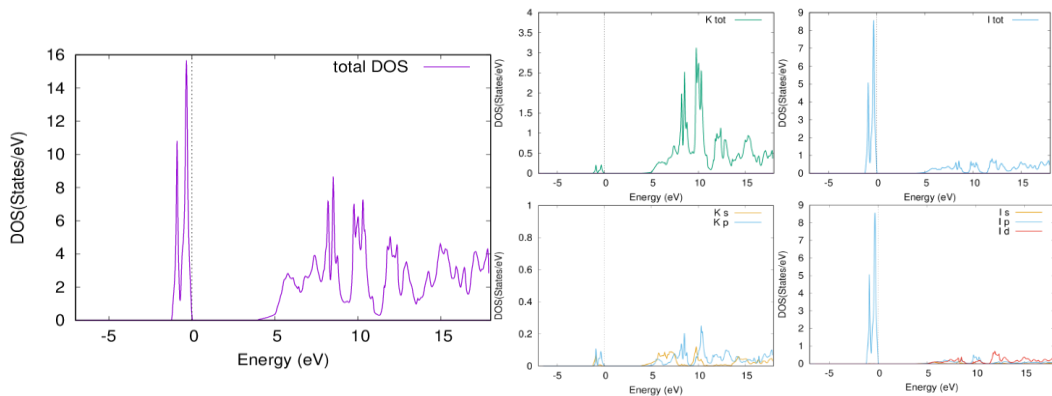


**Figure (5.1.4): Density of states (DOS) of KI in the RS structure, using GGA approximation**

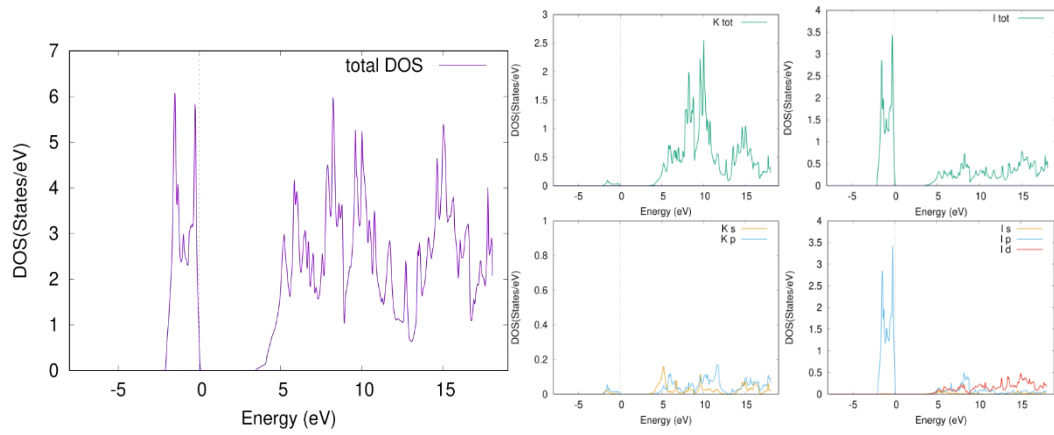


**Figure (5.1.5): Density of states (DOS) of KI in the CsCl structure, using GGA approximation**

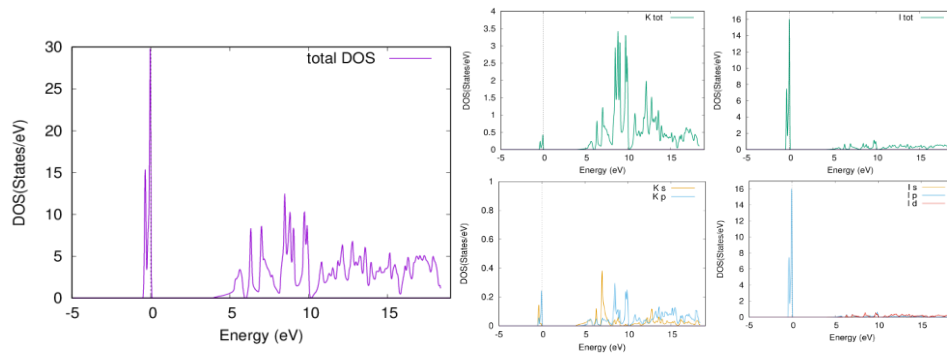


**Figure (5.1.6): Density of states (DOS) of KI in the ZB structure, using GGA approximation**

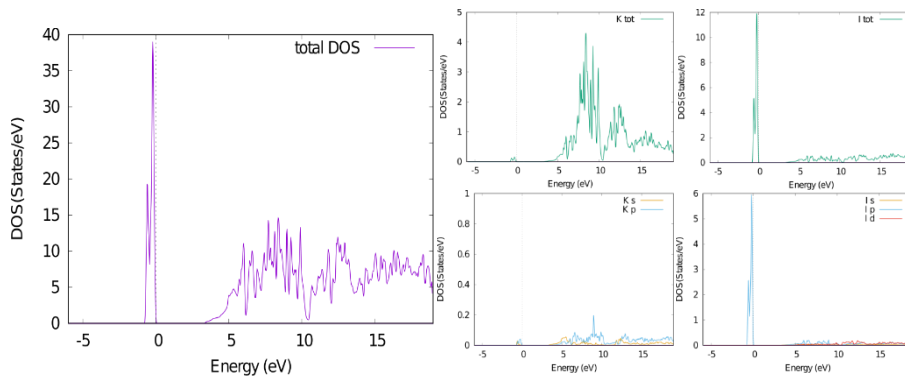


**Figure (5.1.7): Density of states (DOS) of KI in the NiAs structure, using GGA approximation**

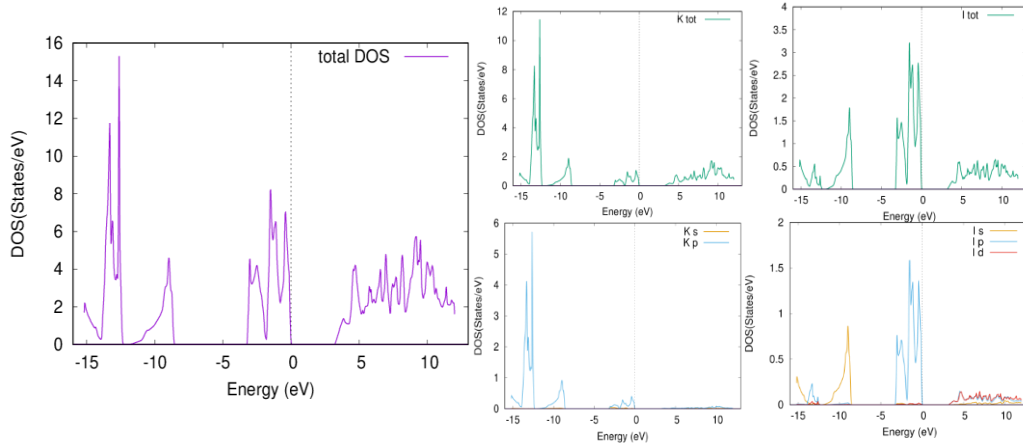


**Figure (5.1.8): Density of states (DOS) of KI in the WZ structure, using GGA approximation**

#### 5.1.4: Elastic properties

The elastic constants as well as the Hill's bulk modulus were calculated and listed in table (5.1.5) for the cubic structures in this study, along with available previous studies results for RS structure. This work's results are in agreement with the other studies.

The elastic constants for KI in RS, CsCl and ZB structures shown in table (5.1.5) and for WZ structure presented in table (5.1.6) satisfy the Born's criteria [66] for stability mentioned in chapter 4. Regarding the bulk modulus, the values are in very good agreement with the results presented in tables (5.1.1) and (5.1.2) using Murnaghan's equation of state [58]. The low values of the bulk modulus for the structures RS, CsCl, ZB and WZ indicate weak resistance to fracturing under pressure. Meanwhile, CsCl is considered

as the hardest structure for KI, as well as the least compressibility ( $\beta=1/B$ ), since it has the highest value of the bulk modulus among other structures. The ZB structure has the least bulk modulus of all the structures, and the highest compressibility.

**Table (5.1.5): The elastic constants ( $C_{11}$ ,  $C_{12}$  and  $C_{44}$ ) and the bulk modulus calculated by Hill's approximation for KI in RS, CsCl and ZB structures, all in (GPa).**

KI	RS			CsCl	ZB
	Elastic constant	This work	Experimental results		
$C_{11}$	24.1738	27.1 <sup>[a]</sup> 33.2 <sup>[b]</sup>	31.7 <sup>[c]</sup>	33.9234	7.5379
$C_{12}$	3.8904	4.5 <sup>[a]</sup> 5.78 <sup>[b]</sup>	3.2 <sup>[c]</sup>	3.1952	6.9166
$C_{44}$	3.8400	3.64 <sup>[a]</sup> 6.2 <sup>[b]</sup>	4.2 <sup>[c]</sup>	2.3456	5.0597
$B_H$	10.651			13.437	7.123

aRef. [24], bRef. [25], cRef. [19]

**Table (5.1.6): The elastic constants ( $C_{11}$ ,  $C_{12}$ ,  $C_{13}$ ,  $C_{33}$  and  $C_{55}$ ) and the bulk modulus calculated by Hill's approximation for KI in WZ structures, all in (GPa)**

KI	WZ
Elastic constant	
$C_{11}$	14.7989
$C_{12}$	5.6100
$C_{13}$	7.9129
$C_{33}$	13.4850
$C_{55}$	3.2262
$B_H$	9.543

The elastic moduli and factors are displayed in table (5.1.7). A material is considered as a completely isotropic material if the anisotropic factor  $A=1$ , and any deviation measures the degree of anisotropy. All the structures: RS,

CsCl and ZB have anisotropic behavior, since none of them have an isotropy of one. On contrary, WZ structure has an isotropy of almost 1, which indicates an isotropic behavior.

**Table (5.1.7): The calculated Hill's Shear modulus ( $S_H$ ), Young's modulus ( $Y_H$ ) in (GPa), Poisson's ratio ( $\nu_H$ ), the anisotropic ratio (A), B/S ratio, Cauchy pressure ( $P_C$ ) in (GPa), the compressibility ( $\beta$ ) in (1/GPa), and the Hardness (H), for KI compound in RS, CsCl, ZB and WZ structures.**

KI	RS	CsCl	ZB	WZ
	This work	This work	This work	This work
$S_H$	5.735	5.55	1.935	3.565
$Y_H$	14.586	14.635	5.322	9.51
$\nu_H$	0.271	0.318	0.375	0.333
A	0.3786	0.1527	16.2875	1.0358
$B_H/S_H$	1.8572	2.4211	3.6811	2.6768
$C_s$	0.0504	0.8496	1.8569	2.3838
$\beta_H$	0.0938	0.7442	0.1404	0.1048
$H_v$	-0.3071	-0.0629	-2.35947	-1.6705

To determine the brittleness or ductility of a material, the (B/S) ratio can be used. All the structures in table (5.1.7) have values of B/S that are higher than 1.75, which shows that KI in those structures has ductile nature. Meanwhile, the shear modulus for the RS is the highest and it is very close to the CsCl structure's shear modulus.

Young's modulus (Y) can be used to study the stiffness of the material, the higher the value of Y, the stiffer the material is. The CsCl structure of KI has the highest value of Y, which suggests that it is the stiffest structure. This is backed up by the fact that the hardness (H) is also the highest for CsCl structure. Meanwhile, the least stiff structure is the ZB, since it has the lowest

Y and H. These results are consistent with the conclusions deduced by the bulk modulus values.

Considering the Cauchy's pressure ( $C_s$ ), all the structures in table (5.1.7) have positive values of the  $C_s$ , this means that the dominant type of bonding is ionic. The RS structure's  $C_s$  has the lowest value which is very close to zero value, as a result, it is fair to say that it has the "highest covalent bonding" of all, but still having ionic bonds as the dominant type of bonding. This is compatible with the Poisson's ratio results, since all values of  $\nu$  are higher than 0.25, indicating ionic bonding within the material.

## **5.2: Rubidium Iodide (RbI) compound**

### **5.2.1: Structural properties**

Table (5.2.1) and table (5.2.2) contain the structural parameters of RbI in the structures RS, CsCl, ZB, NiAs and WZ, including the lattice parameter ( $a$ ), bulk modulus ( $B$ ), and the first pressure derivative of the bulk modulus ( $\dot{B}$ ) for the cubic structures (RS, CsCl and ZB), with the additional lattice parameters: the internal parameter  $u$  for the hexagonal structures (NiAs and WZ). These structural parameters are obtained by fitting the calculated energies at each volume around the equilibrium volume to Murnaghan's equation of state [58]. The equilibrium volume is also found as well as its associated minimum energy. In addition, results from previous work are listed in table (5.2.1). This work's results are consistent with the other studies outputs.

shown in figure (5.2.1). The minimum energy is associated with the RS structure, which indicates that RbI exists in RS structure as the ground state. However, RbI can exist in other structures when the pressure is managed to specific values explained in the next subsection.

**Table (5.2.1): Structural properties of RbI in RS, CsCl and ZB structures with other available experimental and theoretical results.**

RbI Structure	a(opt) (Å <sup>0</sup> )			B(GPa)		Ḃ	V <sub>0</sub> (a.u. <sup>3</sup> )	E <sub>0</sub> (Ry)
	This work	Exp. results	Theo. work	This work	Previous work			
RS	7.5140	7.342 <sup>[a]</sup>	7.342 <sup>[b]</sup> 7.33 <sup>[c]</sup> 7.345 <sup>[d]</sup>	8.8887	11.094 <sup>[e]</sup> 12.2 <sup>[c]</sup> 11.07 <sup>[f]</sup>	4.3021	715.7421	-20201.157504
CsCl	4.4984	4.33 <sup>[g]</sup>	-	10.1560	-	4.5746	614.2950	-20201.149795
ZB	8.3578	-	-	6.1167	-	4.1707	984.9510	-20201.143776

aRef. [86], bRef. [85], cRef. [14], dRef. [23], eRef. [15], fRef. [16], gRef. [12]

**Table (5.2.2): The structural properties of RbI in NiAs and WZ structures**

RbI	NiAs	WZ
Structure		
a=b(opt) (Å <sup>0</sup> )	5.094261	6.162073
c(opt) (Å <sup>0</sup> )	9.255253	8.058759
c/a(opt)	1.8168	1.3078
u(opt)	-	0.499
B(GPa)	8.8182	6.3219
Ḃ	4.3659	4.4184
V <sub>0</sub> (a.u. <sup>3</sup> )/2atoms	714.53275	904.6393
E <sub>0</sub> (Ry)/2atoms	-20201.154107	-20201.147727

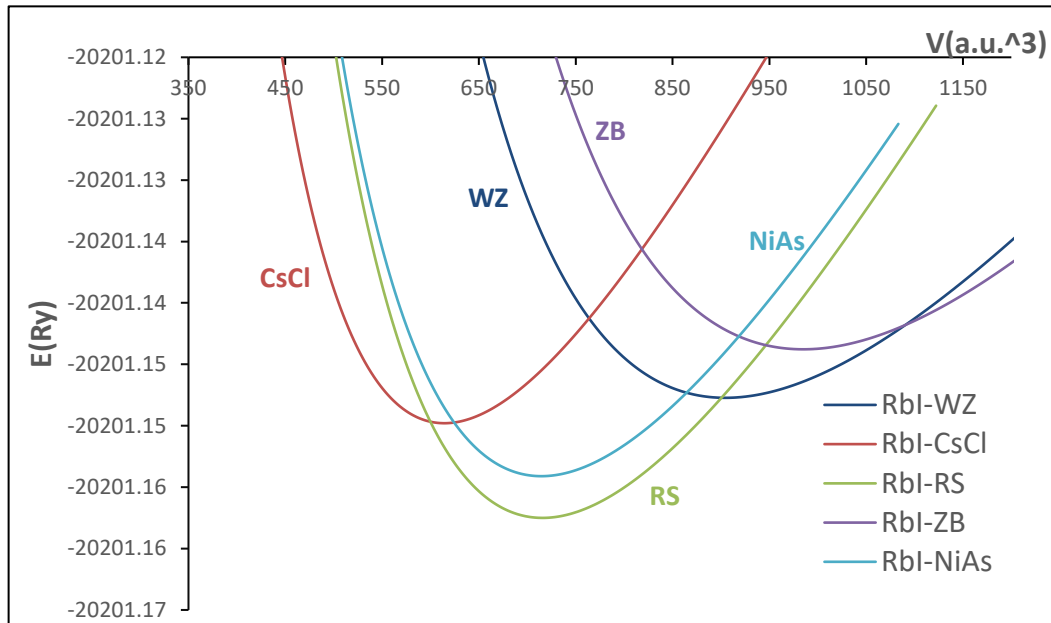


**Figure (5.2.1):** Energy (in Ry) calculated at each volume versus the volume (in a.u.<sup>3</sup>) for RbI in RS, CsCl, ZB, NiAs and WZ structures

### 5.2.2: Phase transition

RbI can transform into other structures than RS by controlling the pressure upon it. The transformations from RS to CsCl and from NiAs to CsCl require a compression process which is associated with positive transition pressure value. In contrary, other transformations such as RS to ZB requires an expansion process that is associated with a negative transition pressure. The enthalpy versus pressure graphs are shown in figure (5.1.2), and the obtained transition pressure values are listed in table (5.2.3).

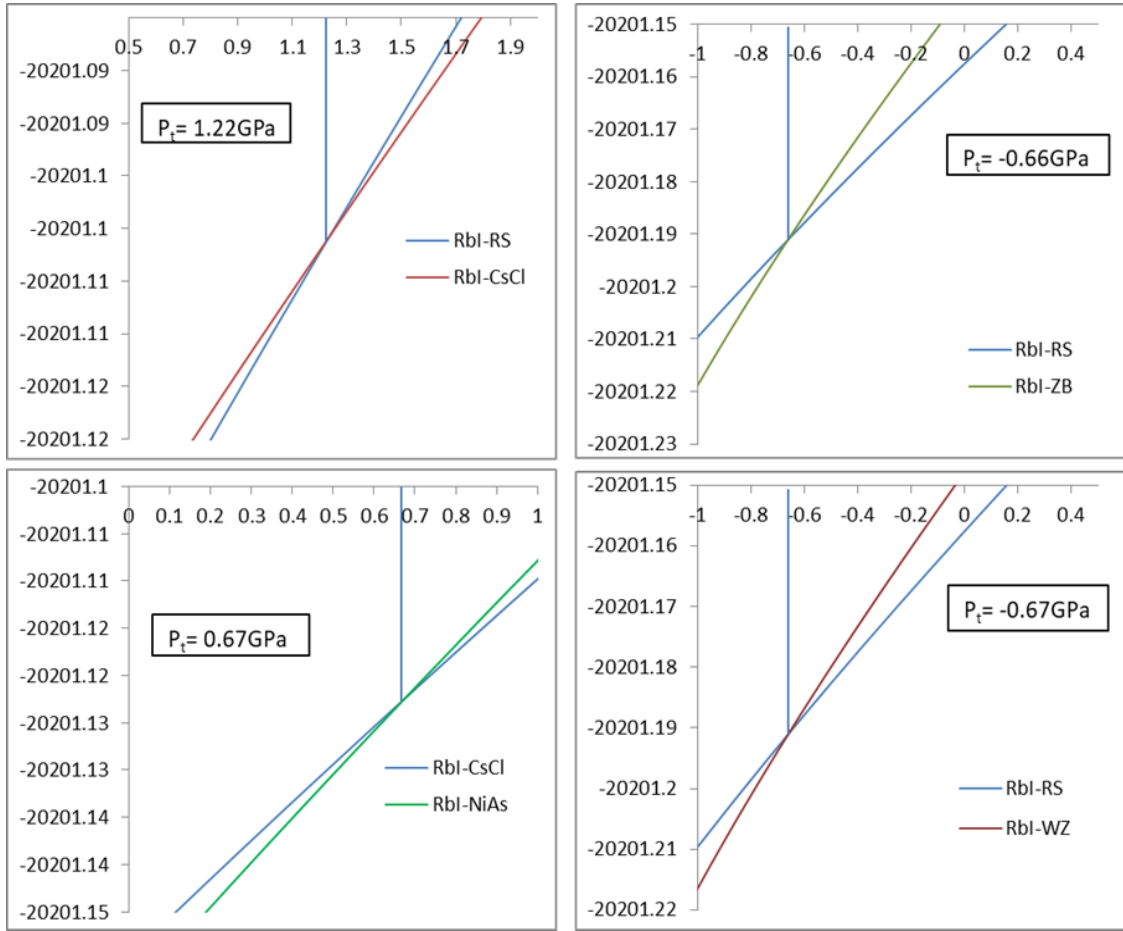


**Figure (5.2.2): Enthalpy  $H$  (in Ry) versus pressure  $P$  (in GPa) for RbI phase transformations using PBE-GGA approximation**

**Table (5.2.3): Transition pressures for the transition of RbI between various structures along other available experimental and theoretical results.**

RbI	RS→CsCl			NiAs→CsCl	RS→ZB	RS→WZ
	This work	Experimental work	Other theoretical results			
Transition pressure	This work	Experimental work	Other theoretical results	This work	This work	This work
$P_t$ (GPa)	1.22	0.35 <sup>[a]</sup> , 0.38 <sup>[b]</sup> 0.4 <sup>[c]</sup>	0.23 <sup>[d]</sup>	0.67	-0.66	-0.67

aRef. [18], bRef. [12], cRef. [5], dRef. [19]

### 5.2.3: Electronic properties

The band structures (BS), shown in figure (5.2.3), were obtained using the PBE-GGA and mBJ-GGA approximations for RbI. The energy is calculated along high symmetry k-points' path and the calculations were done with the optimized lattice constants.

The band gap between the valence and the conduction bands can be seen in the BS graphs.  $E_g$  is calculated as the difference between (MVB) and (MCB) using both: mBJ and GGA approximations and the values are listed in table (5.2.4) along with previous studies' results for the RS structure. Similarly to KI, from figure (5.2.3), it can be observed that RbI in RS, ZB, NiAs and WZ structures, the energy band gap is a direct gap along  $\Gamma$  symmetry line. While in CsCl structure, an indirect energy band gap between  $\Gamma$  and M high symmetry lines can be seen. The GGA approximation underestimates the value of the energy band gap. On the other hand, the results of the mBJ are in good agreement with the other available experimental and theoretical outputs.

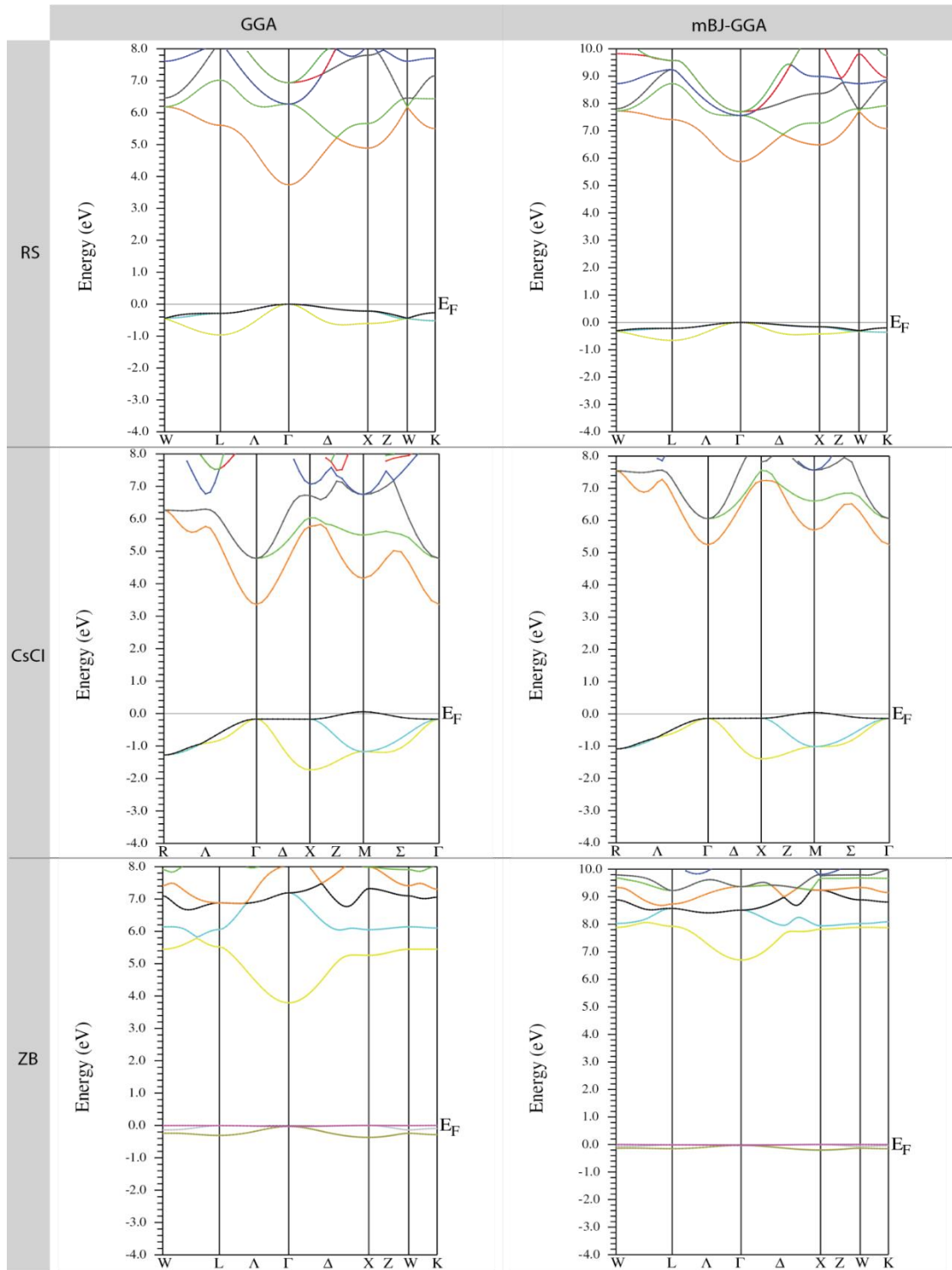


**Figure (5.2.3.a):** Band structures for RbI in the cubic structures RS, CsCl and ZB using the approximation GGA and mBJ.

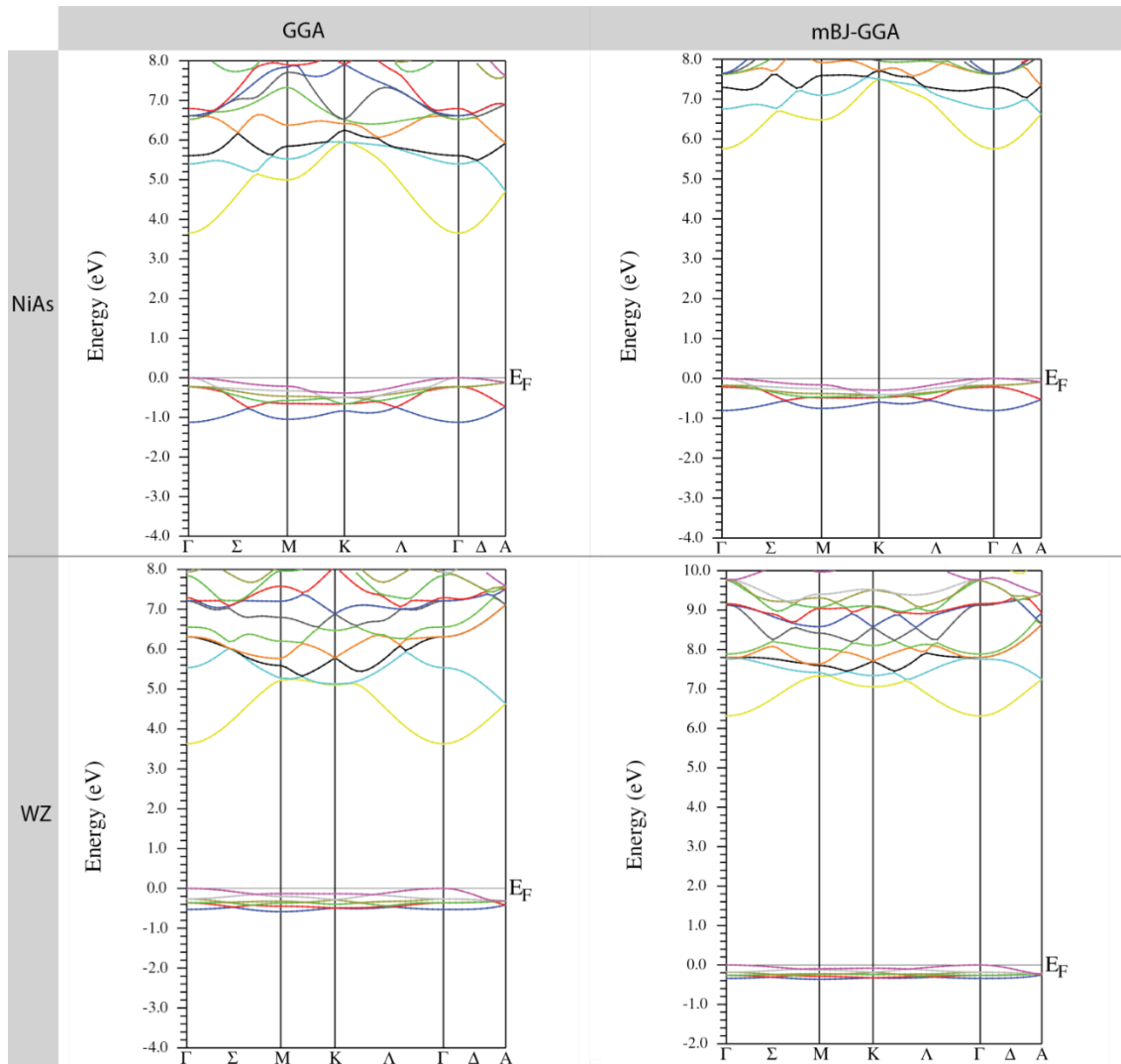


**Figure (5.2.3.b):** Band structure for RbI in the hexagonal structures NiAs and WZ using the approximation GGA and mBJ.

**Table (5.2.4): Energy band gap (in eV) for RbI using GGA and mBJ approximations, with other available experimental and theoretical results.**

RbI											
RS				CsCl		ZB		NiAs		WZ	
This work		Exp. Results	Other theoretical Work	This work		This work		This work		This work	
GGA	mBJ			GGA	mBJ	GGA	mBJ	GGA	mBJ	GGA	mBJ
3.737	5.891	6 <sup>[a]</sup> , 6.3 <sup>[b]</sup>	5.9 <sup>[c]</sup> , 6.028 <sup>[d]</sup> <sub>mBJ</sub>	3.543	5.396	3.791	6.701	3.649	5.753	3.624	6.311

aRef. [20], bRef. [87], cRef. [85], dRef. [23]

The DOS shows the number of states that can be occupied by electrons as a function of energy. The DOS graphs for RbI are shown in figures (5.2.4), (5.2.5), (5.2.6), (5.2.7) and (5.2.8).

Regarding the DOS for RS, CsCl, ZB, and NiAs structures of RbI, they have similar behavior. On the one hand, the DOS for the energies under  $E_F$ , one peak stands the most which is made mainly by iodide p-state, with a small contribution of p and d states of the rubidium. On the other hand, for the energies higher than  $E_F$ , consecutive peaks of DOS can be seen; they are made mainly by the d states in rubidium with a smaller contribution from the iodide d-states.

The DOS for the WZ structure is a bit different. Four peaks can be observed for the energies with values less than  $E_F$ ; the first and third peaks are built by rubidium's p-state with the iodide's s state, while for the second and fourth peaks, the p states in both rubidium and iodide take the lead. The DOS in the

area above  $E_F$  is formed by the contributions of the d-state of rubidium with the d and p states in the iodide.

The energy separation between the conduction and valence states was chosen to be -10 Ry for all the included structures of RbI, except the ZB structure, where the energy separation was chosen to be -8 Ry.

Therefore, the core states for the rubidium are 1s to 3p, while the valence states are from 3d up to 5s for all the included structures in this thesis. For the iodide in the ZB structure, the core states constructed from 1s to 4p states and the valence states from 4d to 5p. However for the iodide in the other structures of RbI, the core states consist of the 1s to 4s states, and the valence states are considered from 4p to 5p states.

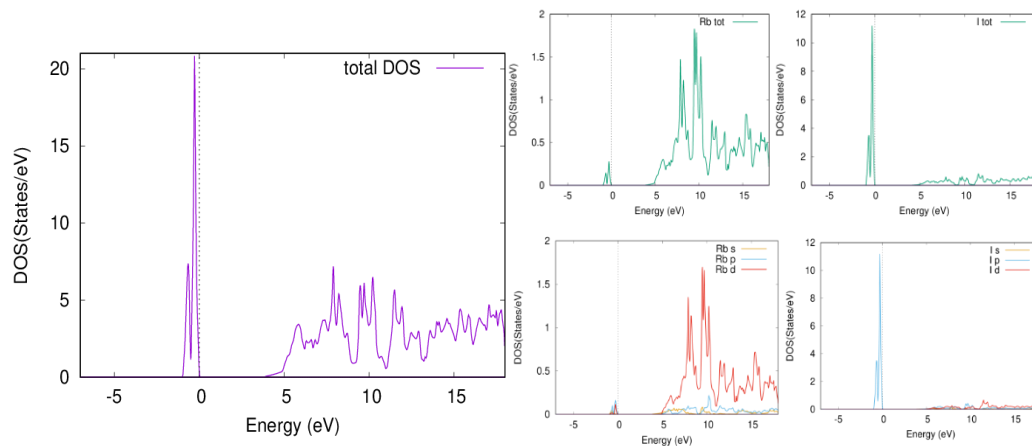


**Figure (5.2.4): Density of states (DOS) for RbI in RS structure using GGA approximation**

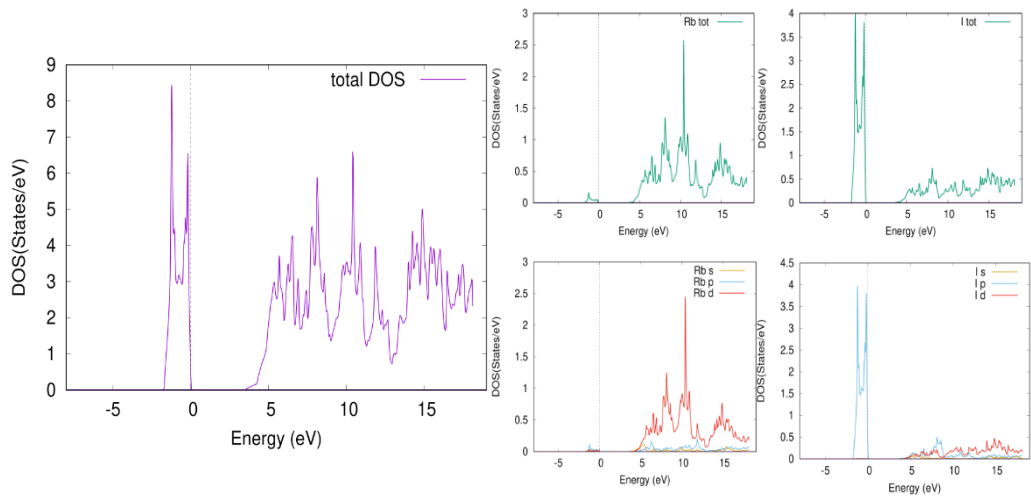


**Figure (5.2.5): Density of states (DOS) for RbI in CsCl structure using GGA approximation**

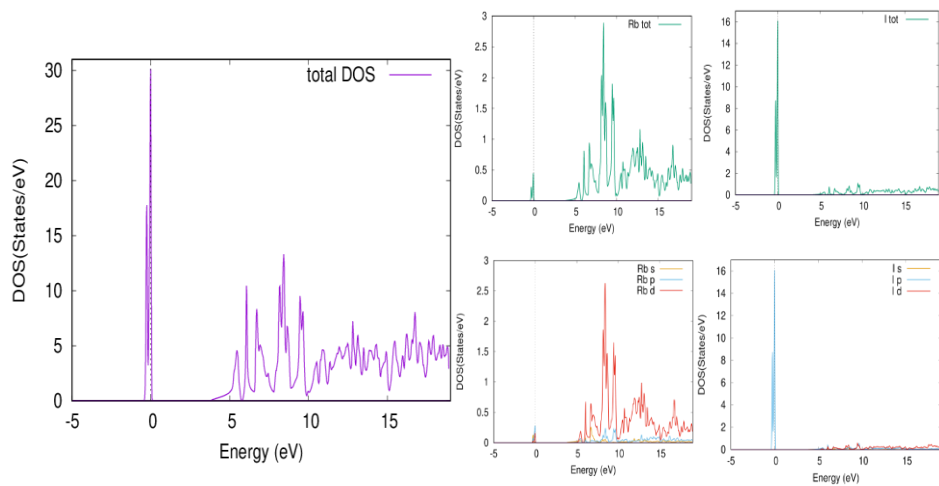


**Figure (5.2.6): Density of states (DOS) for RbI in ZB structure using GGA approximation**

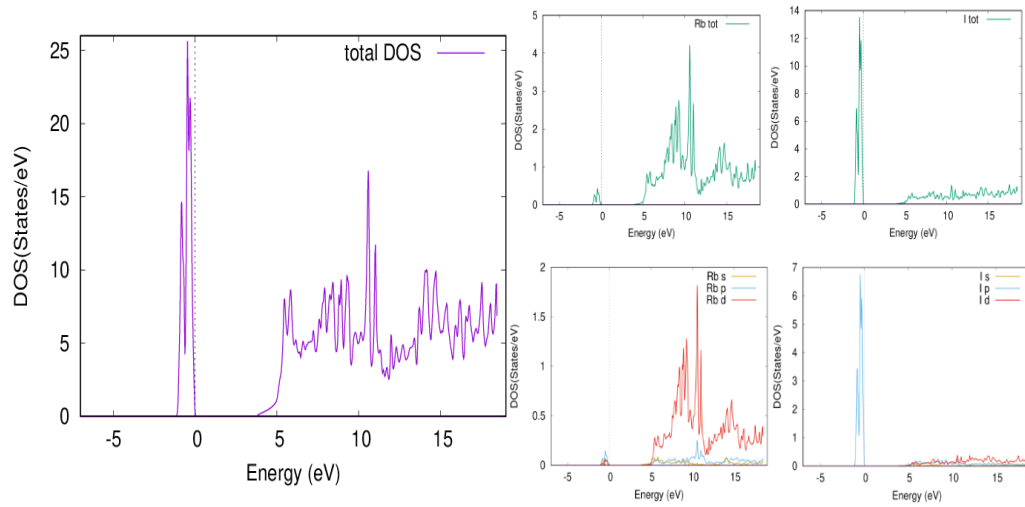


**Figure (5.2.7): Density of states (DOS) for RbI in NiAs structure using GGA approximation**

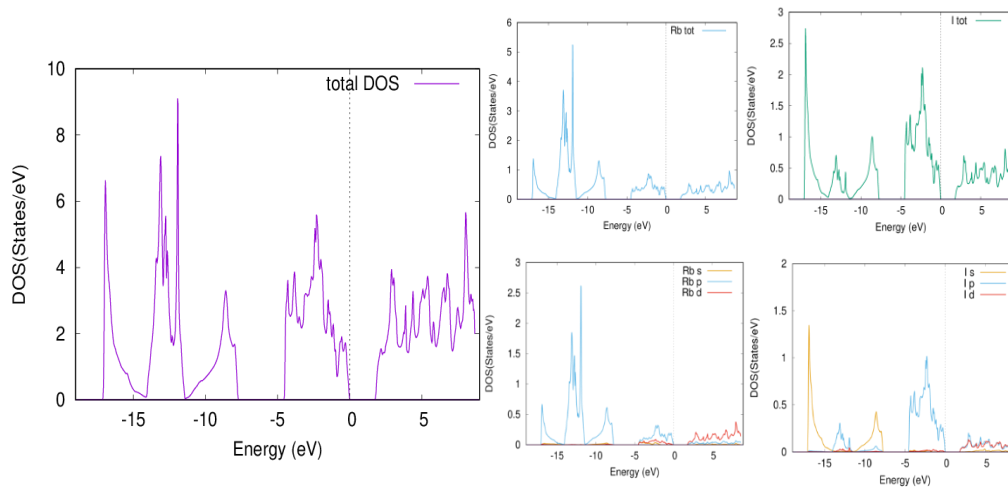


**Figure (5.2.8): Density of states (DOS) for RbI in WZ structure using GGA approximation**

### 5.2.4: Elastic properties

The elastic properties were studied for the optimized lattice parameters and the results are presented in table (4.2.5) for the cubic structures, and table (5.2.6) for the hexagonal structures.

For the cubic structures: RS, CsCl and ZB, Born's criteria for stability were satisfied [66]. As a result, RbI is considered stable in these structures.

Table (5.2.6) shows the elastic constants for RbI in the hexagonal structures: NiAs and WZ. The NiAs structure does not obey the stability conditions since  $c_{55}$  is negative; hence, NiAs is not a stable structure for RbI. Meanwhile, WZ structure satisfies the stability conditions.

**Table (5.2.5): The elastic constants ( $C_{11}$ ,  $C_{12}$  and  $C_{44}$ ) and the bulk modulus calculated by Hill's approximation for RbI in RS, CsCl and ZB structures, all in (GPa).**

RbI	RS			CsCl	ZB
	Elastic constant	This work	Experimental results		
$C_{11}$	20.0554	25.55 <sup>[a]</sup> , 25.5 <sup>[b]</sup> , 25.56 <sup>[c]</sup>	25.8 <sup>[d]</sup>	22.9504	6.4377
$C_{12}$	3.1533	3.45 <sup>[a]</sup> , 3.4 <sup>[b]</sup> , 3.82 <sup>[c]</sup>	3.3 <sup>[d]</sup>	3.5949	6.0774
$C_{44}$	3.1495	2.76 <sup>[a]</sup> , 2.773 <sup>[b]</sup> , 2.78 <sup>[c]</sup>	3.6 <sup>[d]</sup>	2.2535	5.2316
$B_H$	8.787			10.046	6.197

aRef. [18], bRef. [4], cRef. [16], dRef. [19]

**Table (5.2.6): Elastic properties for RbI in NiAs and WZ structures**

RbI	NiAs	WZ
Elastic constant		
$C_{11}$	13.5522	15.8531
$C_{12}$	5.0056	5.5821
$C_{13}$	5.9061	2.3715
$C_{33}$	19.5173	25.6788
$C_{55}$	-30.4302	2.5346
$B_H$	8.763	8.593

The bulk modulus values found using the elastic constants are in excellent agreement with the results presented in tables (5.2.1) and (5.2.2) using

Murnaghan's equation of state [58]. The structures: RS, CsCl, ZB, NiAs and WZ have low values of the bulk modulus; this result in a weak resistance to fracturing. CsCl structure has the highest value of B as well as the least compressibility ( $\beta=1/B$ ), indicating it has the highest resistance to fracturing under stress. On the contrary, the ZB structure has the least bulk modulus of all the structures, and the highest compressibility.

**Table (5.2.7): The calculated Hill's Shear modulus ( $S_H$ ), Young's modulus ( $Y_H$ ) in (GPa), Poisson's ratio ( $\nu_H$ ), the anisotropic ratio (A), B/S ratio, Cauchy pressure ( $P_C$ ) in (GPa), the compressibility ( $\beta$ ) in (1/GPa), and the Hardness (H), for RbI compound in RS, CsCl, ZB and WZ structures.**

RbI	RS	CsCl	ZB	WZ
	This work	This work	This work	This work
$S_H$	4.736	4.237	1.819	4.549
$Y_H$	12.044	11.144	4.97	11.60
$\nu_H$	0.271	0.315	0.366	0.275
A	0.3727	0.2329	29.04	0.4935
$B_H/S_H$	1.8554	2.3710	3.4068	1.8889
$C_s$	0.0038	1.3414	0.8458	3.0475
$\beta_H$	0.1138	0.0995	0.1613	0.1164
$H_v$	-0.5897	-1.3058	-2.3236	-0.6941

Since NiAs structure is found to be unstable, it will not be considered from this point on. Other structures' elastic moduli, factors and ratios are presented in table (5.2.7).

The anisotropic factor for the structures RS, CsCl, ZB and WZ for RbI have values far from unity. This denotes that all of these structures are of anisotropic nature.

Considering the B/S ratio criteria of brittleness and ductility, all B/S values for the structures: RS, CsCl, ZB and WZ are higher than 1.75, indicating the ductile nature of these structures. Meanwhile, the shear modulus for the RS is the highest and the lowest is for ZB structure.

Judging the stiffness using Young's modulus (Y), the higher the Y value, the stiffer the material is. For RbI, the highest value of Y is for RS structure, as a result, RS can be considered the stiffest structure among the structures included for RbI. This is consistent with the hardness (H) values since it is the highest for RS structure.

Considering Cauchy's pressure ( $C_s$ ), all the structures in table (5.2.7) have positive values of the  $C_s$ , which means that the dominant type of bonding is ionic. The RS structure's  $C_s$  has the lowest value which is almost zero. As a result, it is fair to say that it has the "highest covalent bonding nature" of all, but still has ionic bonds as the dominant type of bonding. This is compatible with the Poisson's ratio results, since all values of  $\nu$  are higher than 0.25, indicating ionic bonding within the material.

## Chapter Six

### Conclusion

The compounds potassium iodide (KI) and rubidium iodide (RbI) were investigated in the RS, CsCl, ZB, NiAs and WZ structures using the full-potential linearized augmented plane wave (FP-LAPW) method within density functional theory (DFT) and using the generalized gradient approximation of the potential. This work was done using the WIEN2k package.

The optimized lattice parameters obtained were in good terms with the previous experimental and theoretical results, as well as the values of the bulk modulus. Phase transitions were considered for KI and RbI from RS to CsCl, RS to ZB, and RS to WZ and found to be 2.48, - 0.72, and -0.72 GPa for KI, and 1.22, -0.66, and -0.67 GPa for RbI, respectively. The transition pressure from CsCl into NiAs for KI is found to be -0.84 GPa, and the transition from NiAs to CsCl for RbI demands a transition pressure of 0.67 GPa. The transition from RS to CsCl for both compounds was found to require a compression process as well as the RbI transition from NiAs to CsCl. On the other hand, for the other transitions to occur, the compounds must undergo an expansion process.

The electronic properties were studied using the GGA approximation and enhanced using the modified Becke Johnson (mBJ) approximation. Wider band gaps were achieved using the mBJ, which increased the energy band gap ( $E_g$ ) values to be compatible with the available experimental and theoretical results. The obtained values for  $E_g^{mBJ}$  for the structures RS, CsCl,

ZB, NiAs, and WZ are 5.90, 5.44, 6.65, 5.73, and 6.26 for KI, and 5.89, 5.39, 6.70, 5.75, and 6.31 eV for RbI, in order.

The optimized lattice constants were used to examine the elastic properties. The obtained values of the elastic constants for RS, CsCl, ZB and WZ structures satisfy the Born's stability criteria. In contrast, the RbI in NiAs structure did not meet the stability conditions. The bulk modulus is the highest for the CsCl structure for KI and RbI, indicating stronger resistance to fracturing than other structures, while the lowest value of the bulk modulus was for ZB structure. The Poisson's ratio values were within the range 0.271 to 0.375 and Cauchy pressure values were positive for all the structures included for KI and RbI, this indicates an ionic bonding nature within the lattice.

The hardness is the highest for the CsCl structure of the compound KI and the RS structure for RbI, and the lowest hardness for both compounds is for ZB structure. The stiffness of the materials was judged using Young's modulus. CsCl structure for KI, and RS structure for RbI have the highest values of Young's modulus among other structures, indicating that these structures are the stiffest. On the other hand, ZB had the lowest value of Young's modulus for both compounds, denoting that it is the least stiff structure. The WZ structure for KI has an anisotropic factor of one; hence, it is considered completely isotropic, while all other structures are found to be anisotropic, since the anisotropic factor had values far from unity.

The overall results were found to be compatible with other previous experimental and theoretical outputs.

## References

- [1] Mamula, B. P., Kuzmanović, B., Ilić, M. M., Ivanović, N., and Novaković, N. (2018). Bonding mechanism of some simple ionic systems: Bader topological analysis of some alkali halides and hydrides revisited. *Physica B: Condensed Matter*, 545, 146-151.
- [2] Bessent, R. G., and Runciman, W. A. (1966). Information storage in potassium iodide. *British Journal of Applied Physics*, 17(8), 991.
- [3] Combes, L. S., Ballard, S. S., and McCarthy, K. A. (1951). Mechanical and thermal properties of certain optical crystalline materials. *JOSA*, 41(4), 215-222.
- [4] Lewis, J. T., Lehoczky, A., and Briscoe, C. V. (1967). Elastic constants of the alkali halides at 4.2 K. *Physical Review*, 161(3), 877.
- [5] Asaumi, K., and Mori, T. (1983). High-pressure optical absorption and x-ray-diffraction studies in RbI and KI approaching the metallization transition. *Physical Review B*, 28(6), 3529.
- [6] Teegarden, K. J. (1957). Luminescence of potassium iodide. *Physical Review*, 105(4), 1222.
- [7] Ramola, Y., Louis, C. N., and Amalraj, A. (2017). Pressure Induced Structural Phase Transition, Metallization and Superconductivity in KI. *Chem. Mater. Eng.*, 5(3), 65-74.
- [8] Ramola, Y., Merlinebetsy, J., Louis, C. N., & Amalraj, A. (2019). Pressure Induced Structural Phase Transition, Metallization and Superconductivity in SodiumIodide (NaI). *matrix*, 14, 15.

- [9] Adhikari, G., Adhikari, P., de Souza, E. B., Carlin, N., Choi, S., Djamal, M., and Jeon, E. (2019). An experiment to search for dark matter interactions using sodium iodide detectors. *arXiv preprint arXiv:1906.01791*
- [10] Yam, C., Ma, C., Wang, X., and Chen, G. (2004). Electronic structure and charge distribution of potassium iodide intercalated single-walled carbon nanotubes. *Applied physics letters*, 85(19), 4484-4486.
- [11] Ohlídal, I., and Franta, D. (1997). Rubidium Iodide (RbI). In *Handbook of Optical Constants of Solids* (pp. 857-870). Academic Press.
- [12] Jacobs, R. B. (1938). Polymorphic transitions in metallic halides. *Physical Review*, 54(6), 468.
- [13] Weir, S. T., Akella, J., Aracne-Ruddle, C., Vohra, Y. K., and Catledge, S. A. (2000). Epitaxial diamond encapsulation of metal microprobes for high pressure experiments. *Applied Physics Letters*, 77(21), 3400-3402.
- [14] Cortona, P. (1992). Direct determination of self-consistent total energies and charge densities of solids: A study of the cohesive properties of the alkali halides. *Physical Review B*, 46(4), 2008.
- [15] Chang, Z. P., and Barsch, G. R. (1971). Pressure dependence of the elastic constants of RbCl, RbBr and RbI. *Journal of Physics and Chemistry of Solids*, 32(1), 27-40.

- [16] Ghafelehbashi, M., Dandekar, D. P., and Ruoff, A. L. (1970). Pressure and temperature dependence of the elastic constants of RbCl, RbBr, and RbI. *Journal of Applied Physics*, 41(2), 652-666.
- [17] Barsch, G. R., and Shull, H. E. (1971). Pressure dependence of elastic constants and crystal stability of alkali halides: NaI and KI. *physica status solidi (b)*, 43(2), 637-649.
- [18] Asenbaum, A., Blaschko, O., and Hochheimer, H. D. (1986). Brillouin scattering on rubidium iodide under high pressure. *Physical Review B*, 34(3), 1968.
- [19] Sarkar, A. K., and Sengupta, S. (1969). Many Body Interaction in Alkali Halides. *physica status solidi (b)*, 36(1), 359-364.
- [20] Teegarden, K., and Baldini, G. (1967). Optical absorption spectra of the alkali halides at 10 K. *Physical Review*, 155(3), 896.
- [21] Hopfield, J. J., and Worlock, J. M. (1965). Two-quantum absorption spectrum of KI and CsI. *Physical Review*, 137(5A), A1455.
- [22] Li, J., Duan, C. G., Gu, Z. Q., and Wang, D. S. (1998). Linear optical properties and multiphoton absorption of alkali halides calculated from first principles. *Physical Review B*, 57(4), 2222.
- [23] Bashi, M., Aliabad, H. R., Mowlavi, A. A., and Ahmad, I. (2017). 127I NMR calculations in binary metal iodides by PBE-GGA, YS-PBE0 and mBJ exchange correlation potentials. *Solid state nuclear magnetic resonance*, 82, 10-15.

- [24] Norwood, M. H., and Briscoe, C. V. (1958). Elastic constants of potassium iodide and potassium chloride. *Physical Review*, 112(1), 45.
- [25] Bridgman P. W. (1929). Proc. Am. Acad. Arts Sci. 64, 305
- [26] Gahn, C., and Mersmann, A. (1999). Brittle fracture in crystallization processes Part A. Attrition and abrasion of brittle solids. *Chemical Engineering Science*, 54(9), 1273-1282.
- [27] Schrödinger, E. (1926). Quantisierung als Eigenwertproblem. *Ann Phys*, 79, 361.
- [28] Ceperley, D. M. (1981). The stochastic solution of the many-body Schroedinger equation for fermions. In *Recent Progress in Many-Body Theories* (pp. 262-269). Springer, Berlin, Heidelberg.
- [29] Born M. and Robert Oppenheimer J. 1927. On the Quantum Theory of Molecules. *Annalen der Physik* J 84:457
- [30] Hartree, D. R. (1928, January). The wave mechanics of an atom with a non-Coulomb central field. Part I. Theory and methods. In *Mathematical Proceedings of the Cambridge Philosophical Society* (Vol. 24, No. 1, pp. 89-110). Cambridge university press.
- [31] Fock, V. (1930). Näherungsmethode zur Lösung des quantenmechanischen Mehrkörperproblems. *Zeitschrift für Physik*, 61(1-2), 126-148.
- [32] Hohenberg, P., and Kohn, W. (1964). Inhomogeneous electron gas. *Physical review*, 136(3B), B864.

- [33] Fermi, E. (1927). Statistical method to determine some properties of atoms. *Rend. Accad. Naz. Lincei*, 6(602-607), 5.
- [34] Burke, K., and Wagner, L. O. (2013). DFT in a nutshell. *International Journal of Quantum Chemistry*, 113(2), 96-101.
- [35] Luitz, J. (2006). *Simulation of core level spectra using Density Functional Theory*. na.
- [36] Kohn, W., and Sham, L. J. (1965). Self-consistent equations including exchange and correlation effects. *Physical review*, 140(4A), A1133.
- [37] Von Barth, U., and Hedin, L. (1972). A local exchange-correlation potential for the spin polarized case. i. *Journal of Physics C: Solid State Physics*, 5(13), 1629.
- [38] Slater, J. C. (1972). Statistical exchange-correlation in the self-consistent field. In *Advances in quantum chemistry* (Vol. 6, pp. 1-92). Academic Press.
- [39] Burke, K. (2007). Friends, The ABC of DFT. *Department of Chemistry, University of California, Irvine, CA, 92697*, 117.
- [40] Perdew, J. P. (1986). Density-functional approximation for the correlation energy of the inhomogeneous electron gas. *Physical Review B*, 33(12), 8822.
- [41] Tao, J., Perdew, J. P., Staroverov, V. N., and Scuseria, G. E. (2003). Climbing the density functional ladder: Nonempirical meta-generalized gradient approximation designed for molecules and solids. *Physical Review Letters*, 91(14), 146401.
- [42] Perdew, J. P., Tao, J., Staroverov, V. N., and Scuseria, G. E. (2004). Meta-generalized gradient approximation: Explanation of a realistic

- nonempirical density functional. *The Journal of chemical physics*, 120(15), 6898-6911.
- [43] Perdew, J. P., Burke, K., and Ernzerhof, M. (1996). Generalized gradient approximation made simple. *Physical review letters*, 77(18), 3865.
- [44] Becke, A. D., and Johnson, E. R. (2006). A simple effective potential for exchange. *The Journal of chemical physics*, 124(22), 221101
- [45] Slater, J. C. (1951). A simplification of the Hartree-Fock method. *Physical review*, 81(3), 385.
- [46] Becke, A. D., and Roussel, M. R. (1989). Exchange holes in inhomogeneous systems: A coordinate-space model. *Physical Review A*, 39(8), 3761.
- [47] Tran, F., and Blaha, P. (2009). Accurate band gaps of semiconductors and insulators with a semilocal exchange-correlation potential. *Physical review letters*, 102(22), 226401.
- [48] Jiang, H. (2013). Band gaps from the Tran-Blaha modified Becke-Johnson approach: A systematic investigation. *The Journal of chemical physics*, 138(13), 134115.
- [49] Slater, J. C. (1937). Wave functions in a periodic potential. *Physical Review*, 51(10), 846.
- [50] Andersen, O. K. (1975). Linear methods in band theory. *Physical Review B*, 12(8), 3060.
- [51] Jaradat, R., Abu-Jafar, M., Abdelraziq, I., Omran, S. B., Dahliah, D., and Khenata, R. (2018). High-pressure structural phase transitions and

- electronic properties of the alkali hydride compounds XH (X= K, Rb and Cs). *Materials Chemistry and Physics*, 208, 132-142.
- [52] Blaha, P., Schwarz, K., Sorantin, P., and Trickey, S. B. (1990). Full-potential, linearized augmented plane wave programs for crystalline systems. *Computer physics communications*, 59(2), 399-415.
- [53] Ibach, H., and Lueth, H. (2009). Solid-state physics. An introduction to principles of materials science. 4. ext. upd. and enl.
- [54] Simon, S. H. (2011) Problems for Solid State Physics (3rd Year Course 6) Hilary Term 2011.
- [55] Nelmes, R. J., and McMahon, M. I. (1998). Structural transitions in the group IV, III-V, and II-VI semiconductors under pressure. *Semiconductors and semimetals*, 54, 145-246.
- [56] Abu-Jafar, M., Dayton-Oxland, R., Jaradat, R., Mousa, A. A., and Khenata, R. (2020). Structural, electronic, mechanical and elastic properties of Scandium Chalcogenides by first-principles calculations. *Phase Transitions*, 93(8), 773-783.
- [57] Blaha, P., Schwarz, K., Madsen, G. K., Kvasnicka, D., and Luitz, J. (2001). wien2k. *An augmented plane wave+ local orbitals program for calculating crystal properties*, 60.
- [58] Murnaghan, F. D. (1944). The compressibility of media under extreme pressures. *Proceedings of the national academy of sciences of the United States of America*, 30(9), 244.

- [59] Jaradat, R. (2018). FP-LAPW study of structural, electronic, elastic and optical properties of alkali hydrides compounds XH (X =Li, Na, K, Rb, Cs) [Doctoral dissertation, An-Najah National University].
- [60] Drickamer, H. G., Lynch, R. W., Clendenen, R. L., and Perez-Albueene, E. A. (1967). X-ray diffraction studies of the lattice parameters of solids under very high pressure. In *Solid State Physics* (Vol. 19, pp. 135-228). Academic Press.
- [61] Jaradat, R., Abu-Jafar, M., Abdelraziq, I., Khenata, R., Varshney, D., Omran, S. B., and Al-Qaisi, S. (2017). High-pressure structural phase transition and electronic properties of the alkali hydrides compounds XH (X= Li, Na). *Phase Transitions*, 90(9), 914-927.
- [62] Young, W. C., Budynas, R. G., and Sadegh, A. M. (2002). Roark's formulas for stress and strain (Vol. 7). New York: McGraw-hill
- [63] Wang, J., Yip, S., Phillpot, S. R., and Wolf, D. (1993). Crystal instabilities at finite strain. *Physical review letters*, 71(25), 4182.
- [64] Srinivasan, T. P., and Nigam, S. D. (1969). Invariant elastic constants for crystals. *Journal of Mathematics and Mechanics*, 19(5), 411-420.
- [65] Fast, L., Wills, J. M., Johansson, B., and Eriksson, O. (1995). Elastic constants of hexagonal transition metals: Theory. *Physical Review B*, 51(24), 17431.
- [66] Born, M., Huang, K., and Lax, M. (1955). Dynamical theory of crystal lattices. *American Journal of Physics*, 23(7), 474-474.
- [67] Alers, G. A., and Neighbours, J. R. (1957). Crystal stability and elastic constants. *Journal of Applied Physics*, 28(12), 1514-1514.

- [68] Voigt W. (1889). Over the relationship between the two elasticity constants of isotropic bodies, *Wied. Ann. Phys.* 38:573.
- [69] Reuss A. (1929). Computation of the yield point of mixed crystals due to hiring for single crystals, *Math. Phys.* 9:49.
- [70] Hill R. 1952. The elastic behavior of a crystalline aggregate, *Proc. Phys. Soc. London, Section A* 65:349
- [71] Sanditov, D. S., and Belomestnykh, V. N. (2011). Relation between the parameters of the elasticity theory and averaged bulk modulus of solids. *Technical Physics*, 56(11), 1619-1623.
- [72] Cohen, M. L. (1985). Calculation of bulk moduli of diamond and zinc-blende solids. *Physical Review B*, 32(12), 7988.
- [73] Tan, J., Li, Y., and Ji, G. (2012). Elastic constants and bulk modulus of semiconductors: Performance of plane-wave pseudopotential and local-density-approximation density functional theory. *Computational materials science*, 58, 243-247.
- [74] Ledbetter, H. M. (1977). Elastic properties of zinc: A compilation and a review. *Journal of Physical and Chemical Reference Data*, 6(4), 1181-1203.
- [75] Ledbetter, H. M. (1977). Ratio of the shear and Young's moduli for polycrystalline metallic elements. *Materials Science and Engineering*, 27(2), 133-135.
- [76] Al-Qaisi, S., Abu-Jafar, M. S., Gopir, G. K., Ahmed, R., Omran, S. B., Jaradat, R., and Khenata, R. (2017). Structural, elastic, mechanical and

thermodynamic properties of Terbium oxide: First-principles investigations. *Results in physics* 7, 709-714.

- [77] Pugh, S. F. (1954). XCII. Relations between the elastic moduli and the plastic properties of polycrystalline pure metals. *The London, Edinburgh, and Dublin Philosophical Magazine and Journal of Science*, 45(367), 823-843.
- [78] Chen, X. Q., Niu, H., Li, D., and Li, Y. (2011). Modeling hardness of polycrystalline materials and bulk metallic glasses. *Intermetallics*, 19(9), 1275-1281.
- [79] Yildirim A., Koc H. and Deligoz E. 2012. First-principles study of the structural, elastic, electronic, optical, and vibrational properties of intermetallic Pd<sub>2</sub>Ga, *Chin. Phys.* 21:037101.
- [80] [80] Koval, N. E., Juaristi, J. I., Muiño, R. D., and Alducin, M. (2019). Elastic properties of the TiZrNbTaMo multi-principal element alloy studied from first principles. *Intermetallics*, 106, 130-140.
- [81] Chung, D. H., and Buessem, W. R. (1967). The elastic anisotropy of crystals. *Journal of Applied Physics*, 38(5), 2010-2012.
- [82] Hao, X., Xu, Y., Wu, Z., Zhou, D., Liu, X., and Meng, J. (2008). Elastic anisotropy of OsB<sub>2</sub> and RuB<sub>2</sub> from first-principles study. *Journal of alloys and compounds*, 453(1-2), 413-417.
- [83] Zener C. (1948). *Elasticity and Anelasticity of Metals*, (University of Chicago Press: Chicago).
- [84] Soignard, E., Somayazulu, M., Dong, J., Sankey, O. F., and McMillan, P. F. (2001). High pressure-high temperature synthesis and elasticity

of the cubic nitride spinel  $\gamma$ -Si<sub>3</sub>N<sub>4</sub>. *Journal of Physics: Condensed Matter*, 13(4), 557.

- [85] Van Vechten, J. A. (1969). Quantum dielectric theory of electronegativity in covalent systems. II. Ionization potentials and interband transition energies. *Physical Review* [87] Fröhlich, D., and Stagninus, B. (1967). New assignment of the band gap in the alkali bromides by two-photon spectroscopy. *Physical Review Letters*, 19(9), 496.
- [86] Van Vechten, J. A. (1969). Quantum dielectric theory of electronegativity in covalent systems. I. Electronic dielectric constant. *Physical Review*, 182(3), 891.

جامعة النجاح الوطنية

كلية الدراسات العليا

دراسة الخصائص التركيبية والمرونية والإلكترونية لمركبات  
أيوديد البوتاسيوم وأيوديد الروبيديوم

إعداد

زينب "محمد بكر" "محمد رشدي" معلا

إشراف

أ.د. محمد سلامة أبو جعفر

د. أحمد بصلات

قدمت هذه الرسالة استكمالاً لمتطلبات الحصول على درجة الماجستير في الفيزياء، في  
كلية الدراسات العليا، في جامعة النجاح الوطنية، نابلس – فلسطين.

2021

ب  
دراسة الخصائص التركيبية والمرونية والإلكترونية لمركبات أيوديد البوتاسيوم وأيوديد  
الروبيديوم  
إعداد  
زينب "محمد بكر" "محمد رشدي" معلا  
إشراف  
أ.د. محمد سلامة أبو جعفر  
د. أحمد بصلات

## الملخص

تمت دراسة الخصائص التركيبية والمرونية والإلكترونية لمركبي أيوديد البوتاسيوم وأيوديد الروبيديوم باستخدام طريقة الموجات المستوية المعدلة الخطية للجهد التام (FP-LAPW) وباستخدام تقريب الميل الاتجاهي المعمم للجهد (GGA). وتم استخدام تقريب الميل الاتجاهي المعمم المعدل لبكي وجونسون (mBJ-GGA) لتحسين نتائج الخصائص الإلكترونية.

شملت الدراسة المركبين أيوديد البوتاسيوم و أيوديد الروبيديوم في خمسة تراكيب بلورية وهي: rock-salt (RS) و cesium chloride (CsCl) و Zinblend (ZB) و nickle arsenide (NiAs) و wurtzite (WZ).

لنتائج التي تم الحصول عليها عند دراسة الثوابت التركيبية متوافقة مع النتائج السابقة المتوفرة لدينا، العملية منها والنظرية. كما تشير نتائج بنية حزم الطاقة للمركبين في جميع التراكيب البلورية المدروسة إلى أنها مواد شبه موصلة. بالإضافة لأن التركيب البلوري (RS) أكثر التراكيب البلورية استقراراً لكلا المركبين.

تمت دراسة الخصائص المرونية وحساب الثوابت المرونية للتراكيب البلورية (RS) rock-salt و cesium chloride (CsCl) و Zinblend (ZB) و wurtzite (WZ)، وعند تطبيق معايير بورن لاستقرار المركبات تبين أن هذه التراكيب مستقرة لأيوديد البوتاسيوم وأيوديد الروبيديوم، بينما أشارت قيم الثوابت المرونية لمركب أيوديد الروبيديوم بتراكيب (NiAs) nickle arsenide إلى أنه تركيب غير دلت قيم الثوابت المرونية على طبيعة مرنة لجميع التراكيب المستقرة، كما أشارت إلى أن تركيب (CsCl) هو التركيب الأكثر صلابة لأيوديد البوتاسيوم، لكن تركيب (RS) هو الأكثر صلابة لأيوديد الروبيديوم.